

**МІНІСТЕРСТВО ОСВІТИ І НАУКИ УКРАЇНИ
НАЦІОНАЛЬНИЙ АВІАЦІЙНИЙ УНІВЕРСИТЕТ
КАФЕДРА КОНСТРУКЦІЇ ЛІТАЛЬНИХ АПАРАТІВ**

ДОПУСТИТИ ДО ЗАХИСТУ
Завідувач кафедри, д.т.н., проф.
_____ Сергій ІГНАТОВИЧ
«____» _____ 2022

ДИПЛОМНА РОБОТА
ВИПУСКНИКА ОСВІТНЬОГО СТУПЕНЯ МАГІСТРА
ЗІ СПЕЦІАЛЬНОСТІ
«АВІАЦІЙНА ТА РАКЕТНО-КОСМІЧНА ТЕХНІКА»

Тема: «Розрахунок геометрії черв'ячної передачі і аналіз її міцності»

Виконавець: _____

Сянцюань Цзен

Керівник: д.т.н., професор _____

Михайло КАРУСКЕВИЧ

Охорона праці: к.т.н., доцент _____

Катерина КАЖАН

Охорона навколишнього середовища: _____

Лариса ЧЕРНЯК

Нормоконтролер: к.т.н., доцент _____

**Володимир
КРАСНОПОЛЬСЬКИЙ**

Київ 2022

**MINISTRY OF EDUCATION AND SCIENCE OF UKRAINE
NATIONAL AVIATION UNIVERSITY
DEPARTMENT OF AIRCRAFT DESIGN**

APPROVED BY

Head of department Dr. of Sc., prof.
____ Sergiy IGNATOVICH
"___" _____ 2022

**MASTER THESIS
ON SPECIALITY
"AVIATION AND SPACE ROCKET TECHNOLOGY"**

Theme: "Worm gear transmission geometry calculation and its strength analysis"

Prepared by: _____ **Xiangquan ZENG**

Supervisor: Dr. of Sc., professor _____ **Mykhailo KARUSKEVYCH**

**Labor protection:
Ph.D., associate professor** _____ **Katerina KAZHAN**

**Environmental protection:
Ph.D., associate professor** _____ **Larisa CHERNYAK**

**Standards Inspector:
Ph.D., associate professor** _____ **Volodymyr
KRASNOPOLSKYI**

Kyiv 2022

НАЦІОНАЛЬНИЙ АВІАЦІЙНИЙ УНІВЕРСИТЕТ

Факультет аерокосмічний

Кафедра конструкції літальних апаратів

Освітній ступінь «Магістр»

Спеціальність 134 «Авіаційна та ракетно-космічна техніка»

Спеціалізації «Обладнання повітряних суден»

ЗАТВЕРДЖУЮ

Завідувач кафедри д.т.н., проф.

Сергій ІГНАТОВИЧ

« » 2022

ЗАВДАННЯ

на виконання дипломної роботи студента

Сянцюань ЦЗЕН

1. Тема роботи «Розрахунок геометрії черв'ячної передачі і аналіз її міцності», затверджена наказом ректора від 05 жовтня 2022 року № 1861/ст.
2. Термін виконання проекту: з 06 жовтня 2022 р. по 30 листопада 2022 р.
3. Вхідні дані до проекту: характеристики черв'ячної передачі.
4. Зміст пояснівальної записки: пояснівальна записка з аналізом стану проблеми, розрахунки і 3D моделювання, математичні моделі, аналіз напружено-деформованого стану.
5. Перелік обов'язкового графічного (ілюстративного) матеріалу: 3D креслення черв'ячної передачі, результати параметричного моделювання CATIA V5, результати ANSYS аналізу міцності. Графічні матеріали виконані в CATIA V5, ANSYS Workbench.
6. Календарний план-графік

№	Завдання	Термін виконання	Відмітка про виконання
1	Отримання завдання, обробка статистичних даних або аналіз сучасних ідей, концепцій, дизайнів	05.10.2022 – 12.10.2022	

2	Теоретичне дослідження черв'ячних торцевих передач зі сміщенням і побудова математичних моделей	13.10.2022 – 14.10.2022	
3	Розрахунки, побудова 3D-моделі	15.10.2022 – 28.10.2022	
4	Аналіз згинальних напружень на об'єкті дослідження, узагальнення закономірностей	28.10.2022 – 3.11.2022	
5	Використання CATIA для параметричного моделювання	03.11.2022 – 7.11.2022	
6	Використання ANSYS для виконання аналізу на міцність моделі	07.11.2022 – 12.11.2022	
7	Завершення пояснлювальної записки	12.11.2022 – 15.11.2022	

7. Консультанти з окремих розділів

Розділ	Консультанти	Дата, підпис	
		Завдання видав	Завдання прийняв
Охорона праці	Катерина КАЖАН		
Охорона навколишнього середовища	Лариса ЧЕРНЯК		

8. Дата видачі завдання: «___» 2022 р.

Керівник дипломної роботи _____ Михайло КАРУСКЕВИЧ

Завдання прийняв до виконання _____ Сянцюань ЦЗЕН

NATIONAL AVIATION UNIVERSITY

Faculty aerospace

Department of aircraft design

Master's degree

Specialty 134 "Aviation and space rocket technology"

Educational professional program "Aircraft equipment"

APPROVED BY

Head of Department, Dr. of Sc., prof.

_____ Sergiy IGNATOVYCH

"___" _____ 2022

TASK

For the master degree thesis

Xiangquan ZENG

1. Topic «Worm gear transmission geometry calculation and its strength analysis», approved by the Rector's order № 1861/ct of 05 October 2022.
2. Thesis terms: from 5th October 2022 to 30th November 2022.
3. Initial data: characteristics and parameters of the involute cylindrical worm and face gear.
4. Content: face gear tooth geometry, face gear tooth contact stress analysis, face gear tooth bending stress analysis.
5. Required material: explanatory notes with state of the art analysis, calculations, and 3D model; stress-strain analysis, presentation of the results.
6. Thesis schedule:

№	Task	Time limits	Done
1	Obtaining the task, processing statistical data or analysis of contemporary ideas, concepts, designs	05.10.2022 – 12.10.2022	
2	Theoretical study of offset worm face gears and construction of mathematical models	13.10.2022 – 14.10.2022	

3	Calculations, Building a 3D model	15.10.2022 – 28.10.2022	
4	Analysis of the bending stresses on the object of study, summarizing the laws	28.10.2022 – 3.11.2022	
5	Parametric modelling with CATIA	03.11.2022 – 07.11.2022	
6	Strength analysis of the model by using ANSYS Workbench	07.11.2022 – 12.11.2022	
7	Completion of the explanatory note	12.11.2022 – 15.11.2022	

7. Special chapter consultants

Chapter	Consultants	Date, signature	
		Task issued	Task received
Labor protection	Katherina KAZHAN		
Environmental protection	Larisa CHERNYAK		

8. Date: "___" _____ 2022

Supervisor of diploma work _____ Mykhailo KARUSKEVYCH

Task for execution is given for _____ Xiangquan ZENG

РЕФЕРАТ

Магістерська робота «Розрахунок геометрії черв'ячної передачі і аналіз її міцності»

85 с., 33 рис., 4 табл., 39 джерел

Торцева передача – це новий тип передачі, який має багато унікальних переваг, особливо у високошвидкісних і важких умовах. У роботі досліджено генерацію поверхні зуба та характеристики зачеплення зубчастих коліс із зміщеною поверхнею, моделювання обробки зубчастих передач із зміщеною поверхнею та аналіз динаміки приводів із зміщеною поверхнею.

Створено математичну модель евольвентного оффсетного циліндричного черв'ячного приводу. Завдяки аналізу характеристик зачеплення торцевої зубчастої передачі отримано рівняння траєкторії контакту поверхні зуба торцевої шестерні та поверхні зуба циліндричного черв'яка.

Тривимірна модель черв'ячної зубчастої передачі зі зсувом створюється та збирається на основі програмного забезпечення SolidWorks, а потім імпортується в програмне забезпечення ABAQUS для кінцево-елементного аналізу. Досліджено контактні лінії та контактні сліди зсувної черв'ячної торцевої передачі; отримано спричинену поверхнею зуба нормальну кривизну контактних точок, а еліптичні довгі та короткі осі та значення контактної напруги точкового контакту зміщеної черв'ячної шестерні розраховуються за допомогою теорії Герца, теоретичні розрахунки перевіряються за допомогою програмного забезпечення кінцевих елементів. Потім проаналізовано згиальне напруження черв'ячної передачі зі зміщенням при навантаженні одним зубом і отримано закон зміни напружень згину.

Запропоновано конструкцію зубів оффсетної черв'ячної передачі.

Зсуvinий циліндричний черв'ячний привід, торцевий привід, геометричний розрахунок, аналіз міцності, динамічний аналіз

ABSTRACT

Master degree thesis "Worm gear transmission geometry calculation and its strength analysis"

85 pages, 33 figures, 4 tables, 39 references

Face gearing is a new type of gearing that has many unique advantages, especially in high-speed, heavy-duty applications. The paper investigates the tooth surface generation and meshing characteristics of offset face gears, machining modelling of offset face gear drives and dynamics analysis of offset face gear drives.

The mathematical model of the involute offset cylindrical worm drive is established. Through the analysis of the meshing characteristics of the face gear transmission, the contact trajectory equations of the face gear tooth surface and the cylindrical worm tooth surface are derived.

Three-dimensional model of the offset worm face gear transmission is created and assembled based on SolidWorks software, then imported into ABAQUS software for finite element analysis. The contact lines and contact traces of the offset worm face gear transmission are investigated; the tooth surface induced normal curvature of the contact points is derived; and the elliptical long and short axes and contact stress values of the point contact of the offset worm face gear are calculated using Hertzian theory, and the theoretical calculations are verified using finite element software. Then, the bending stresses of the offset worm face gear with single tooth loading are analysed and the bending stress variation law is derived.

The tooth design of the offset worm face gear is proposed.

Offset cylindrical worm drive, face gear drive, geometric calculation, strength analysis, dynamic analysis

CONTENT

ABBREVIATIONS	11
INTRODUCTION	12
PART 1. THE INTRODUCTION OF OFFSET WORM FACE GEAR TRANSMISSION	13
1.1 Research background and significance	13
1.2 The transmission characteristics of face gear	14
1.3 The characteristics of Offset worm face gear transmission	17
1.4 The research status of face gear transmission	18
Conclusion for part 1.....	19
PART 2. ACCURATE PARAMETRIC MODELING OF OFFSET WORM FACE GEAR	20
2.1 Establishment of offset cylindrical worm space coordinate system and coordinate transformation.....	20
2.2 Establishment of 3D model of Offset worm face gear	34
Conclusion for part 2.....	44
PART 3. STRENGTH ANALYSIS OF OFFSET WORM FACE GEARS	45
3.1 Determine the meshing point coordinate value	45
3.2 Surface gear contact stress calculation.....	46
3.3 Finite element calculation of single tooth contact stress of tooth surface gear	51
3.4 Offset worm face gear loading meshing analysis	55
Conclusion for part 3.....	66
PART 4. Labor protection	67
4.1 Hazard factors	67
4.2 Prevention and Control Measures	70
4.3 Fire safety rules for work areas.....	72
Conclusion of part 4	77
PART 5. ENVIROMENT PROTECTION	78
5.1 Environmental impact of metal machining processes	78
5.2 Pollution to the environment caused by metal machining process	79

5.3 Specific countermeasures to prevent pollution in the metal machining process	79
5.4 Contamination prevention plan for parts cleaning fluid cleaning process	83
Conclusion of part 5	85
REFERENCES	86

ABBREVIATIONS

ICAO – International Civil Aviation Organization;

EASA – European Union Aviation Safety Agency;

FAA – Federal Aviation Administration;

FAR – Federal Aviation Regulations;

FG – Face gearing

OCWG – Offset cylindrical worm gear;

MC – Meshing characteristics

INTRODUCTION

Contemporary aircraft, particularly cargo planes are equipped with loading and unloading mechanisms, for example, winches, hoists, onboard cranes, transporters, etc.

The different kinds of gears are integrated into the design of aircraft machines.

The objective of this paper is to geometrically design and 3D model the worm and face teeth in a transmission scheme with offset worm face teeth and to analysis the strength of the gears during meshing. In order to achieve this, the following objectives are specified:

- Analysis of the latest research on worm-face gearing;
- Investigation deficiencies in worm-face gearing;
- As the investigation identified root cut, side cut and short cut problems in spur worm face gears, offset worm face gearing was proposed to avoid these problems;
- Theoretical analysis of offset worm face gearing and derivation of the relevant equations;
- Determination of the relevant parameters of the worm and face gears and the establishment of a mathematical model of the gears;
- Determine the method to achieve the objective - build a 3D model and perform stress-strain analysis.

PART 1. THE INTRODUCTION OF OFFSET WORM FACE GEAR TRANSMISSION

1.1 Research background and significance

In modern machinery and equipment of all kinds of transmission forms, gear transmission compact structure, high transmission efficiency, good reliability, long life and other characteristics, so that it has become the most widely used form of mechanical transmission, large to industrial development in the power transmission of aerospace equipment, small to daily life in all kinds of instrumentation pointer rotation, gear transmission plays a vital role. To a certain extent, gear transmission is related to and marks the level of development of the national machinery industry, is one of the key concerns of engineering researchers [1]. With the change in the working environment and working conditions of gears, gear research is also in progress, its type has experienced the development of cylindrical gears, bevel gears, worm gears, face gears, its tooth shape has also experienced the development of straight teeth, helical teeth, herringbone teeth, spiral teeth, arc teeth, etc.

Face gearing is a relatively new type of gearing, evolving from bevel gears, which become face gears when the tooth surface of the bevel gear is distributed on a circular plane [2]. Compared to bevel gears, face gears have the following advantages: no axial force, which simplifies support and reduces the weight of the system structure, making it possible to adapt to a wider range of occasions; single-stage transmission ratio can reach 20:1, with a high degree of overlap, greatly improving the smoothness of the transmission; compact structure, strong load-bearing capacity, gear box mass is greatly reduced, therefore, in-depth research on face gears is essential to improve the Therefore, in-depth research on the face gear is of great importance to improve the thrust-to-weight ratio and reliability of the aviation transmission system [3]. Worm drive is a combination of worm wheel and worm, commonly used to transmit the motion and power between two staggered shafts, can be seen as the evolution of the spiral gear or spiral drive, with a large ratio, compact structure, smooth operation, low noise, as well as no other auxiliary institutions that can be obtained without the transmission of the advantages of self-locking

reverse stroke. It is commonly used in the interlocking of two shafts, the transmission ratio is large, the transmission power is not too large or intermittent work occasions.

Offset cylindrical worm drive is a new type of worm drive, offset means that the working spiral of the worm is placed on one side of the worm wheel, compared with the positive cylindrical worm drive, the worm is offset to avoid the problem of root cutting, cutting edge and short cutting in the transmission process [4]. In this transmission method, as the worm is cylindrical, the tooth shape of the face gear must be curved, as opposed to straight and helical face gears, the tooth shape of the curved face gear is curved, and thus the overlap of the transmission pair will be further increased during the transmission process. At the same time there is practice shows that, compared with the traditional worm drive, offset cylindrical worm drive high efficiency, offset worm can be used as the active transmission parts; compared with the bevel gear drive, has the advantages of small weight, small vibration, transmission ratio, low noise [5]. However, at present, the domestic research on the offset worm face gear transmission vice is not very common, and most of the current published literature focuses on the meshing principle of other types of face gears and the application of face gear transmission in the aviation field, which directly affects the further optimization and promotion of this transmission form, especially in the application of high speed and heavy load and other demanding occasions, therefore, it is necessary to carry out research on this new worm drive model. It is therefore necessary to study this new worm gear model.

1.2 The transmission characteristics of face gear

Face gear transmission is a gear transmission that meshes cylindrical gear and bevel gear. Fig. 1.1 is the face gear transmission, where the gear 1 is an ordinary straight cylindrical gear (pinion) and gear 2 is the face gear (bevel gear). The axes of the two wheels intersect and the Angle between them is γ . The offset cylindrical worm drive studied in this paper is the case of face gear drive when $\gamma = 90^\circ$, and the drive shafts are spatially staggered and the worm shaft axis is not in the conventional worm shaft section as shown in fig. 1.2.

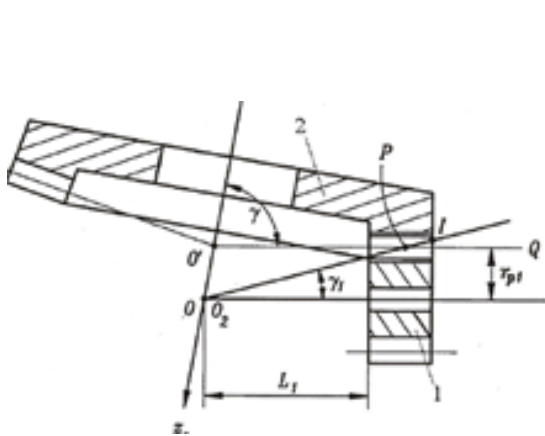


Fig. 1.1. Diagram of face gearing.

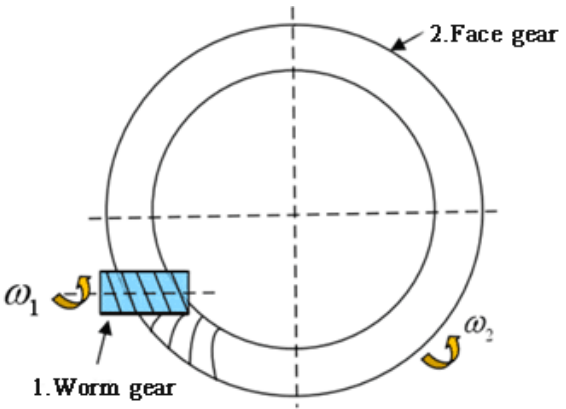


Fig. 1.2. Offset worm face gear transmission.

In order to enable the face gearing to mesh properly, the bevel gears are not normal bevel gears, but are machined using the same size gear insert as the cylindrical gears they are mated to by the Conjugate method. As this gear mechanism achieves transmission between intersecting shafts, it is similar to an ordinary bevel gear transmission with a beveled pitch surface. The meshing angle varies with the position on the tooth width and is constant for a given position. At positions where the radius of the pitch bevel of the pinion is equal to the radius of the base circle of the cylindrical gear, the meshing angle becomes 0.

However, the tooth width of a face gear cannot reach a position where the mesh angle is equal to 0. In fact, around this point, the top transition of the tool cuts off the conjugate profile of the face gear during the cutting process, i.e. root cutting occurs. At the point where the pitch cone radius of the pinion is equal to the index circle radius of the cylindrical gear, the angle of engagement is the pressure angle of the index circle. The farther away from the axis of the face gear, the greater the meshing angle and the smaller the top thickness of the tooth. At a certain position, the top thickness of the tooth of the face gear is 0, producing a cusp phenomenon. Therefore, one end of the tooth of the face gear is easy to root cut, and the other end of the tooth The top of the tooth will become sharp, making its tooth width limited to a certain extent, affecting its load-bearing capacity.

Face gear transmission has many unique advantages and geometric phenomena[6]. Compared with bevel gear transmission, face gear transmission has the following advantages [7-8]:

1. The pinion is an involute cylindrical gear, whose axial position error has almost no effect on transmission performance.

Other directions (such as radial) the impact of error is also relatively small, without anti-location error design; and in the ordinary bevel gear drive, the two bevel gear cone tops to coincide, axial error will cause serious off-load phenomenon. In some important bevel gear drive (such as aviation spiral bevel gear drive) but also special anti-location error (i.e. to prevent the separation of the cone top) design. As a result, the installation time of the face gearing mechanism is greatly reduced and only the axial position of the face worm gear needs to be adjusted.

2. The face gear drive has a greater degree of overlap than an ordinary bevel gear drive. According to the relevant literature, the degree of recombination under no load can generally reach $1.6 \sim 1.8$, theoretically the degree of recombination can be as high as 2.0 above, in the load will be higher. It is quite important to improve the load carrying capacity and increase the smoothness of transmission.

3. When the pinion is a straight cylindrical gear, there is no axial force acting on the pinion. This simplifies the support, reduces weight and correspondingly increases the load carrying capacity. This is extremely useful for applications where space is restricted and light weight is required.

4. The pinion is an involute gear, which by the nature of the involute is known to have the same common normal of the simultaneously meshed tooth pairs and does not change at different moments. This is extremely advantageous for power transmission.

5. For point contact surface gear transmission, in theory can still ensure the fixed transmission ratio transmission. The commonly used point contact bevel gear drive from the principle has not been able to ensure a fixed transmission ratio drive, its transmission ratio is in a certain range of fluctuations. So it is smaller vibration and lower noise than the face gear transmission.

According to the traditional view, the shortcomings of face gear transmission mainly have two aspects:

1. Since the dimensions of the tool for machining the face gear are the same as those of the cylindrical gear in the actual mesh, it is, in Theoretically, the tool for machining the

face gears is manufactured separately, which is costly and takes a long time to manufacture.

2. The tooth width of the face gear cannot be designed to be too long due to the limitations of root cutting and tooth apex sharpening, thus the load-bearing capacity of the face gear is limited.

The offset cylindrical worm drive studied in this paper is essentially a combination of an involute helical gear with a small number of teeth and a face gear. The transmission is also known as a worm because of the small number of teeth in the involute worm. This transmission differs by:

1. The worm is more flexible in its position.
2. The worm has a smaller number of teeth and a larger transmission ratio.
3. Variations in worm gear tooth shape will be beneficial to the formation of a variety of tooth shape meshing transmission.
4. Transmission design parameters are simple, and its contact performance is better than that of face gears.
5. Large degree of overlap and strong load carrying capacity.

1.3 The characteristics of Offset worm face gear transmission

The offset cylindrical worm drive can be seen as an evolution of or a special case of the following drives.

One is the evolution of the traditional worm drive. That is, in the traditional worm gearing, if the worm wheel is moved along its axis by a distance, the worm gear tooth surface is distributed along its end face, and the worm shaft axis is offset in space on the worm gear tooth surface. The axis of the worm gear is offset in space to one end of the worm gear tooth surface. In terms of the meshing principle, this means that the offset worm gear tooth surface is an extension of the conventional worm gear tooth surface. The offset worm gear face is an extension of the conventional worm gear face. Therefore, it is possible to apply the traditional method of worm gear mesh analysis to the study of offset worm gearing. In this transmission analysis, the worm gear tooth face is common.

In another case, it can be considered as an evolution of bevel gearing. That is, the large bevel gear evolves into a bevel angle of 90° for the face gears, while the small bevel gear evolves into a cylindrical gear with a bevel angle of zero degrees. It appears that the common offset cylindrical worm is essentially a common helical gear with a smaller number of teeth.

Combining the above two cases, the offset cylindrical worm drive can also be viewed in the context of a bevel worm drive, i.e. in a bevel worm drive. That is, in the case of a bevel worm drive [9], the taper angle of the bevel worm wheel tends to 90° , while the taper angle of the bevel worm tends to zero, and set the tooth surface of the tapered worm to normal.

The offset cylindrical worm drive is a transmission consisting of a common cylindrical gear with a small number of teeth and a face worm wheel, so this form of transmission has the advantage of a large transmission ratio of worm gears, but also has the characteristic of a high efficiency bevel gear transmission. The drive has the advantage of a large ratio of worm gears and a high efficiency of bevel gears. The drive is therefore not self-locking and the face worm gear can be used as the active part.

1.4 The research status of face gear transmission

The study of face gears dates back to the early days, the most representative being Buckingham's introduction of face gearing in his book 'Analytical mechanics of gears' in 1949 [10]. The basic idea is that the teeth of a face gear are regarded as a rack of teeth with variable pressure angle and variable pitch. In the 1950s, Emilio and Dornig investigated the phenomenon of root tangency in face gears with orthogonal axes [11]. O.E proposed a face gear with a threaded cylindrical (or beveled) worm (Face Worm Gear); Litvin carried out further in-depth research on this method. This gearing has a large degree of overlap, improved meshing properties compared to face and cylindrical gearing, and increased the ability of the gear to transmit loads and smoothness of transmission. The method can be used not only for intersecting shaft drives, but also for staggered shaft drives.

In 1955, Emilo had two very important papers on face gears, the first of which he wrote jointly with Dornig and which concentrated on geometry and kinematics. The second paper concentrated on the root cut. However, the analysis in both articles was limited to orthogonal axes and standard involute gears. O.E., published in 1954 and 1960 [12], proposed a face gear and threaded cylindrical or bevel worm gear transmission. This was a major contribution to the development of face gears and the greatest advantage of this type of transmission is the large degree of overlap. This type of gear has the advantage that several pairs of gears are in contact at the same time during the meshing process.

This type of face gearing was further investigated at the end of the last century and the beginning of this century, with Goldfarb's publications in 1999 and 2000 and Dudas's in 2000 being the most representative.

Over the last 20 years, Litvin and his institute have made important contributions to the study of face gears. Litvin has studied the meshing of face gears [13], on the one hand obtaining conditions for root tangency and tooth apex cusps based on differential geometry and meshing principles, and on the other hand developing point contact face gears. With the development of computer simulation, these two aspects of research have been further developed. Computer simulations of face-mesh transmissions have shown that assembly errors can cause contact point deflections without affecting transmission errors. In China, in 2016, Lijie Hu parametrically modeled offset worm face gears [14]; in 2019, Qing Li et al. simulated the machining of worm face gears in VERICUT to verify the feasibility of the flying tool machining method for worm face gears [15].

Conclusion for part 1.

1. Introduces the development and emergence of face gears and explains the background and significance of the research in this thesis.

2. Introduces the characteristics of face gears and offset worm gear drives.

Briefly reviews some research literatures related to face gears.

PART 2. ACCURATE PARAMETRIC MODELING OF OFFSET WORM FACE GEAR

In the process of finite element analysis, the geometric model of the gear will directly affect the accuracy and convergence of the analysis, therefore, before carrying out the finite element analysis of the face gear, an accurate model of the gear needs to be established. The face shape and meshing process of the offset worm face gear are more complex, so the difficulty of modelling is higher than that of the general face gear. In this paper, based on the gear meshing theory, the relevant tooth equations of the face gear are derived, and then the discrete point coordinates of the left and right sides of the face gear are solved by MATLAB to find the contact line of the tool tooth surface, and then the tooth surface curve is fitted. After obtaining the tooth face equations of the face gear, the 3D model is then built using SolidWorks. The parametric modelling of the modified and unmodified offset worm face gear in this chapter lays the foundation for the subsequent finite element analysis.

The content of this chapter is arranged as follows: firstly, establish the spatial coordinate system for the offset cylindrical worm gear; secondly, derive the basic equations, such as the offset worm spiral equation, etc.; finally, derive the meshing equations for the offset cylindrical worm gearing, the worm gear tooth equation and the mesh boundary line equation formed during the meshing of the worm gearing.

2.1 Establishment of offset cylindrical worm space coordinate system and coordinate transformation

2.1.1 Establishing a spatial coordinate system

The offset worm face gear transmission coordinate system ^[16] is established as shown in the fig.2.1, where:

$S_w = [O_w; i_w, j_w, k_w]$ is a fixed coordinate system with the worm in a rotary motion around the k_w axis;

$S_f = [O_f; i_f, j_f, k_f]$ is a fixed coordinate system with the worm in a rotary motion around the k_f axis;

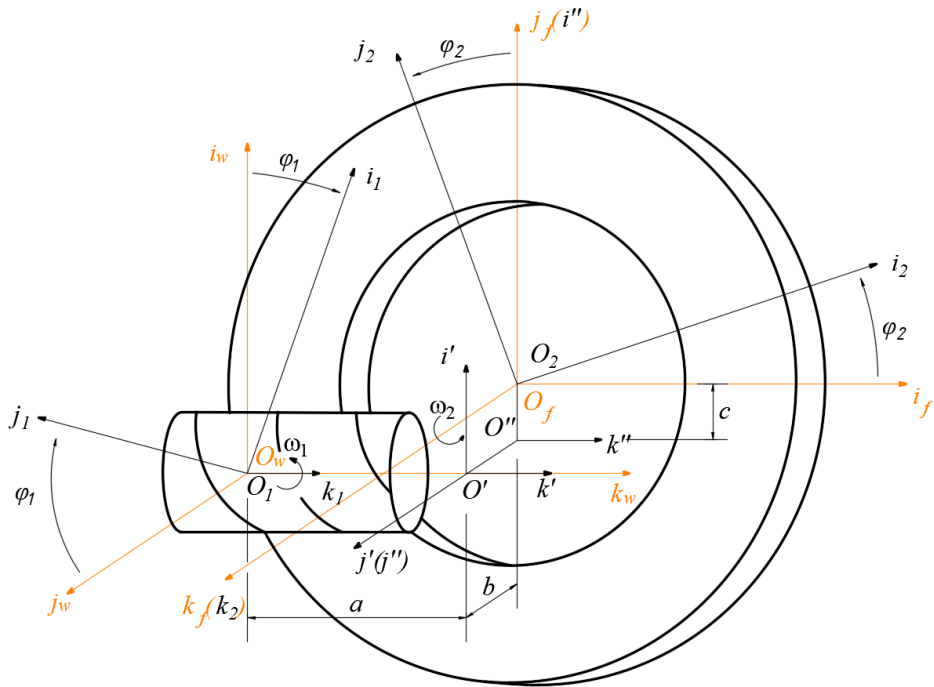


Fig. 2.1. Offset cylindrical worm drive space coordinate system.

$S' = [O'; i', j', k']$ is the transition coordinate system, obtained by moving the coordinate system S_w by a lengths in the positive direction of the k_w axis.

$S'' = [O''; i'', j'', k'']$ is the transition coordinate system, obtained by moving the coordinate system S' by b lengths in the positive direction of the j' axis.

$S_1 = [O_1; i_1, j_1, k_1]$ is the dynamic coordinate system, fixed to the worm, which remains relatively stationary with respect to the worm teeth during transmission, φ_1 is the angle at which the worm is rotated.

$S_2 = [O_2; i_2, j_2, k_2]$ is the dynamic coordinate system, fixed to the worm, which remains relatively stationary with respect to the worm teeth during transmission, φ_2 is the angle at which the worm is rotated.

2.1.2 Coordinate transformation

Fixed coordinate system S_w [17] is obtained by rotating φ_1 counterclockwise around the k_w axis in the dynamic coordinate system S_1 , the transformation matrix M_{w1} can be solved for between its coordinate systems is:

$$\mathbf{M}_{wI} = \begin{bmatrix} \cos \varphi_1 & \sin \varphi_1 & 0 & 0 \\ -\sin \varphi_1 & \cos \varphi_1 & 0 & 0 \\ 0 & 0 & 1 & 0 \\ 0 & 0 & 0 & 1 \end{bmatrix}$$

Fixed coordinate system S' is obtained by moving the coordinate system S_w by a lengths in the positive direction of the k_w axis, the transformation matrix $M_{w'}$ can be solved for between its coordinate systems is:

$$\mathbf{M}_{w'} = \begin{bmatrix} 1 & 0 & 0 & 0 \\ 0 & 1 & 0 & 0 \\ 0 & 0 & 1 & -a \\ 0 & 0 & 0 & 1 \end{bmatrix}$$

Fixed coordinate system S'' is obtained by moving the coordinate system S' by a lengths in the positive direction of the j' axis, the transformation matrix $M_{w''}$ can be solved for between its coordinate systems is:

$$\mathbf{M}_{w''} = \begin{bmatrix} 1 & 0 & 0 & 0 \\ 0 & 1 & 0 & b \\ 0 & 0 & 1 & 0 \\ 0 & 0 & 0 & 1 \end{bmatrix}$$

Fixed coordinate system S_f is obtained by translating the fixed coordinate system S'' by c units in the positive direction along the i'' axis, then rotating 90°clockwise around the k'' axis and then 90°clockwise around the i'' axis, the transformation matrix $M_{fw''}$ can be solved for between its coordinate systems is:

$$\mathbf{M}_{fw''} = \begin{bmatrix} 0 & 1 & 0 & -c \\ 0 & 0 & 1 & 0 \\ 1 & 0 & 0 & 0 \\ 0 & 0 & 0 & 1 \end{bmatrix}$$

Dynamic coordinate system S_2 is obtained by rotating φ_2 counterclockwise around the k_f axis in the dynamic coordinate system S_f , the transformation matrix M_{2f} can be solved for between its coordinate systems is:

$$\mathbf{M}_{2f} = \begin{bmatrix} \cos \varphi_2 & \sin \varphi_2 & 0 & 0 \\ -\sin \varphi_2 & \cos \varphi_2 & 0 & 0 \\ 0 & 0 & 1 & 0 \\ 0 & 0 & 0 & 1 \end{bmatrix}$$

Multiplying the above transformation matrix together gives the transformation matrix M_{21} from the coordinate system S_1 where the worm is located to the coordinate system S_2 where the face gear is located as

$$\begin{aligned} \mathbf{M}_{21} &= \mathbf{M}_{2f} \mathbf{M}_{fw''} \mathbf{M}_{w''} \mathbf{M}_{w'} \mathbf{M}_{w1} \\ &= \begin{bmatrix} -\cos \varphi_2 \sin \varphi_1 & \cos \varphi_1 \cos \varphi_2 & \sin \varphi_2 & b \cos \varphi_2 - c \cos \varphi_2 - a \sin \varphi_2 \\ \sin \varphi_1 \sin \varphi_2 & -\cos \varphi_1 \sin \varphi_2 & \cos \varphi_2 & c \cos \varphi_2 - b \sin \varphi_2 - a \sin \varphi_2 \\ \cos \varphi_1 & \sin \varphi_1 & 0 & 0 \\ 0 & 0 & 0 & 1 \end{bmatrix} \end{aligned}$$

2.1.3 Basic equations

Involute equation. As shown in the fig.2.2, the coordinate system $O_w X_w Y_w$ is established in the worm shaft section. The line MN makes a roll along the base circle, the radius of the base circle is r_b , and the trajectory \widehat{ef} travelled by the point N is the involute. In the coordinate system $O_w X_w Y_w$, the starting point of the involute on the right-hand side of the worm gear groove is e.

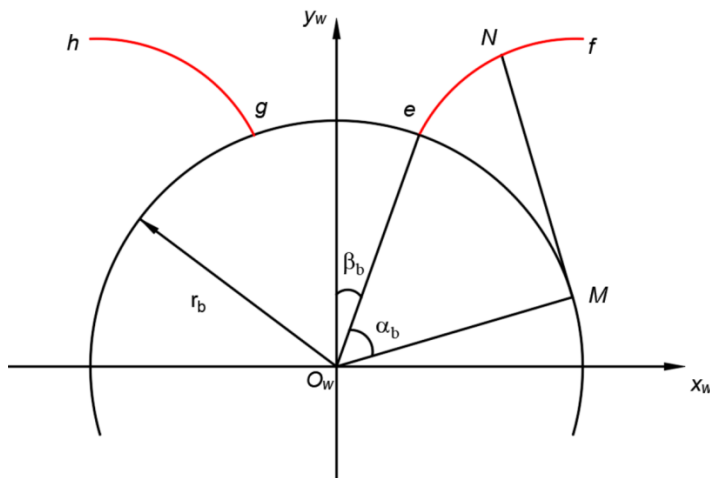


Fig. 2.2. Involute of worm cross-section.

The angle between $O_w e$ and the y_w axis is β_b . Any point N is taken on the involute and made tangent to the base circle past the point N . The tangent point is $O_w e$ and $O_w M$ is

α_b . It varies with the point N . According to the nature of the involute, we know that $MN = \widehat{eM} = \alpha_b r_b$, which gives the involute \widehat{ef} equation:

$$\begin{cases} \mathbf{r}_R^w = x_{wR} \mathbf{i} + y_{wR} \mathbf{j} \\ x_{wR} = r_b \sin(\beta_b + \alpha_b) - r_b \alpha_b \cos(\beta_b + \alpha_b) \\ y_{wR} = r_b \cos(\beta_b + \alpha_b) + r_b \alpha_b \sin(\beta_b + \alpha_b) \end{cases} \quad (2.1)$$

We can also get the equation the involute \widehat{gh} equation:

$$\begin{cases} \mathbf{r}_L^w = x_{wL} \mathbf{i} + y_{wL} \mathbf{j} \\ x_{wL} = -r_b \sin(\beta_b + \alpha_b) + r_b \alpha_b \cos(\beta_b + \alpha_b) \\ y_{wL} = r_b \cos(\beta_b + \alpha_b) + r_b \alpha_b \sin(\beta_b + \alpha_b) \end{cases} \quad (2.2)$$

Involute surface equation. The face of the worm can be seen as the result of the spiral movement of the helix gg' tangent to the base cylinder around the axis of the worm, which is formed as shown in fig. 2.3.

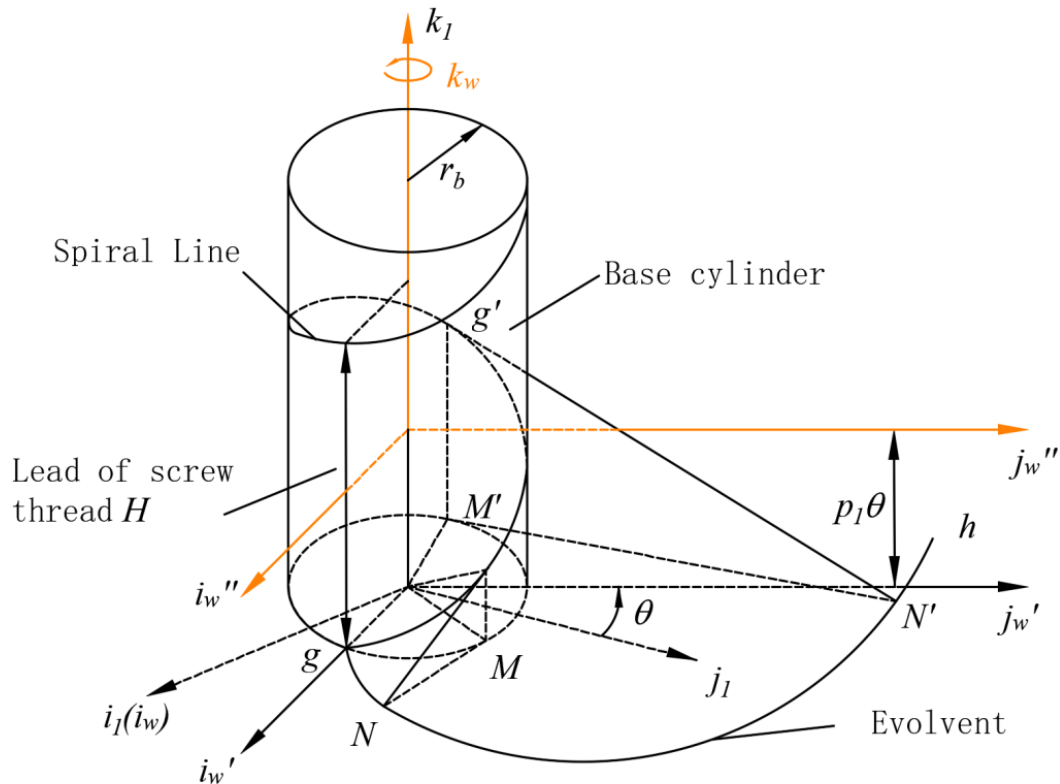


Fig. 2.3. The formation of an involute spiral surface.

Assume that the involute \widehat{gh} is established in the fixed coordinate system $S_1 = [O_1; i_1, j_1, k_1]$, and that there is relative motion of the fixed coordinate system S_w to the dynamic coordinate system $S_1 = [O_1; i_1, j_1, k_1]$: the angular velocity of the fixed

coordinate system S_w relative to the dynamic coordinate system S_1 at while rotating uniformly counterclockwise about the k_w axis and moving uniformly along the k_w direction. When S_w rotates by an angle of θ , its coordinate origin moves a distance of $p_1\theta$ along the k_w direction, where $p_1 = H/2\pi$, p_1 is the spiral parameter, H is the lead of screw thread, and the involute \widehat{gh} formed by this form of motion is the right-hand spiral surface of the worm.

The coefficient matrix \mathbf{M}_{1w} of any point $N(x_w, y_w, z_w)$ on the involute \widehat{gh} transformed from the coordinate system S_w to S_1 is:

$$\mathbf{M}_{1w} = \begin{bmatrix} \cos \theta & -\sin \theta & 0 & 0 \\ \sin \theta & \cos \theta & 0 & 0 \\ 0 & 0 & 1 & p_1\theta \\ 0 & 0 & 0 & 1 \end{bmatrix}$$

From $\mathbf{r}_L^I = \mathbf{M}_{1w} \cdot \mathbf{r}_L^w$, we can get:

$$\begin{cases} \mathbf{r}_L^I = x_{1L}\mathbf{i}_1 + y_{1L}\mathbf{j}_1 + z_{1L}\mathbf{k}_1 \\ x_{1L} = x_{wL} \cos \theta - y_{wL} \sin \theta \\ y_{1L} = x_{wL} \sin \theta + y_{wL} \cos \theta \\ z_{1L} = z_{wL} + p_1\theta \end{cases} \quad (2.3)$$

Substituting the involute \widehat{gh} equation (2.2) gives:

$$\begin{cases} \mathbf{r}_L^I = x_{1L}\mathbf{i}_1 + y_{1L}\mathbf{j}_1 + z_{1L}\mathbf{k}_1 \\ x_{1L} = -r_b \sin(\beta_b + \alpha_b + \theta) + r_b \alpha_b \cos(\beta_b + \alpha_b + \theta) \\ y_{1L} = r_b \cos(\beta_b + \alpha_b + \theta) - r_b \alpha_b \sin(\beta_b + \alpha_b + \theta) \\ z_{1L} = p_1\theta \quad (z_{wL} = 0) \end{cases} \quad (2.4)$$

Let $\tau = \beta_b + \alpha_b + \theta$, then the equation of the tooth surface on the left side (right side of the tooth) of the involute cylindrical worm gear tooth groove is:

$$\begin{cases} \mathbf{r}_L^I = x_{1L}\mathbf{i}_1 + y_{1L}\mathbf{j}_1 + z_{1L}\mathbf{k}_1 \\ x_{1L} = -r_b \sin \tau + r_b \alpha_b \cos \tau \\ y_{1L} = r_b \cos \tau + r_b \alpha_b \sin \tau \\ z_{1L} = p_1(\tau - \beta_b - \alpha_b) \end{cases} \quad (2.5)$$

Same reason substituting the involute \widehat{ef} equation (2.1), the equation of the tooth surface on the right side (left side of the tooth) of the involute cylindrical worm gear tooth groove is:

$$\begin{cases} \mathbf{r}_L^I = x_{1R}\mathbf{i}_1 + y_{1R}\mathbf{j}_1 + z_{1R}\mathbf{k}_1 \\ x_{1R} = r_b \sin(\beta_b + \alpha_b - \theta) - r_b \alpha_b \cos(\beta_b + \alpha_b - \theta) \\ y_{1R} = r_b \cos(\beta_b + \alpha_b - \theta) + r_b \alpha_b \sin(\beta_b + \alpha_b - \theta) \\ z_{1R} = p_1 \theta \quad (z_{wR} = 0) \end{cases} \quad (2.6)$$

Let $\tau' = \beta_b + \alpha_b - \theta$, the equation is:

$$\begin{cases} \mathbf{r}_R^I = x_{1R}\mathbf{i}_1 + y_{1R}\mathbf{j}_1 + z_{1R}\mathbf{k}_1 \\ x_{1R} = r_b \sin \tau' - r_b \alpha_b \cos \tau' \\ y_{1R} = r_b \cos \tau' + r_b \alpha_b \sin \tau' \\ z_{1R} = p_1 (\beta_b + \alpha_b - \tau') \end{cases} \quad (2.7)$$

Unit normal vector equation for any point on the face of an involute worm [18].

Assuming that the unit normal vector \mathbf{n} points from the inside of the worm to the outside of the worm, the tangential vector at any point on the worm tooth lies in the plane defined by the coordinate vectors $\frac{\partial \mathbf{r}^1}{\partial \alpha_b}$ and $\frac{\partial \mathbf{r}^1}{\partial \tau}$, so the equation for the normal vector \mathbf{n} at that point is:

$$\mathbf{n} = \frac{\frac{\partial \mathbf{r}^1}{\partial \alpha_b} \times \frac{\partial \mathbf{r}^1}{\partial \theta}}{\left| \frac{\partial \mathbf{r}^1}{\partial \alpha_b} \times \frac{\partial \mathbf{r}^1}{\partial \theta} \right|} = \frac{\begin{vmatrix} \mathbf{i}_1 & \mathbf{j}_1 & \mathbf{k}_1 \\ \frac{\partial \mathbf{x}}{\partial \alpha_b} & \frac{\partial \mathbf{y}}{\partial \alpha_b} & \frac{\partial \mathbf{z}}{\partial \alpha_b} \\ \frac{\partial \mathbf{x}}{\partial \theta} & \frac{\partial \mathbf{y}}{\partial \theta} & \frac{\partial \mathbf{z}}{\partial \theta} \end{vmatrix}}{\left| \frac{\partial \mathbf{r}^1}{\partial \alpha_b} \times \frac{\partial \mathbf{r}^1}{\partial \theta} \right|} = n_{x_1} \mathbf{i}_1 + n_{y_1} \mathbf{j}_1 + n_{z_1} \mathbf{k}_1$$

In the formula: $\mathbf{n}_{x_1}, \mathbf{n}_{y_1}, \mathbf{n}_{z_1}$ are the components of the normal vector \mathbf{n} on the X_1, Y_1, Z_1 axes.

The unit normal vector in the coordinate system S_1 at any point on the left-hand tooth surface of the worm is:

$$\mathbf{n}_L^1 = \frac{\frac{\partial \mathbf{r}_L^I}{\partial \alpha_b} \times \frac{\partial \mathbf{r}_L^I}{\partial \theta}}{\left| \frac{\partial \mathbf{r}_L^I}{\partial \alpha_b} \times \frac{\partial \mathbf{r}_L^I}{\partial \theta} \right|} = n_{x_1 L} \mathbf{i}_1 + n_{y_1 L} \mathbf{j}_1 + n_{z_1 L} \mathbf{k}_1$$

In the formula:

$$\begin{cases} \frac{\partial \mathbf{r}_L^I}{\partial \alpha_b} = -r_b \alpha_b \cos \tau \mathbf{i}_1 + r_b \alpha_b \sin \tau \mathbf{j}_1 + 0 \mathbf{k}_1 \\ \frac{\partial \mathbf{r}_L^I}{\partial \theta} = [-r_b \cos \tau - r_b \alpha_b \sin \tau] \mathbf{i}_1 + (-r_b \sin \tau + r_b \alpha_b \cos \tau) \mathbf{j}_1 + p_1 \mathbf{k}_1 \end{cases}$$

$$\frac{\partial \mathbf{r}_L^I}{\partial \alpha_b} \times \frac{\partial \mathbf{r}_L^I}{\partial \theta} = \begin{vmatrix} \mathbf{i}_1 & \mathbf{j}_1 & \mathbf{k}_1 \\ \frac{\partial \mathbf{x}_1}{\partial \alpha_b} & \frac{\partial \mathbf{y}_1}{\partial \alpha_b} & \frac{\partial \mathbf{z}_1}{\partial \alpha_b} \\ \frac{\partial \mathbf{x}_1}{\partial \theta} & \frac{\partial \mathbf{y}_1}{\partial \theta} & \frac{\partial \mathbf{z}_1}{\partial \theta} \end{vmatrix} = \alpha_b p_1 r_b \cos \tau \mathbf{i}_1 + \alpha_b p_1 r_b \sin \tau \mathbf{j}_1 + \alpha_b r_b^2 \mathbf{k}_1$$

$$\left| \frac{\partial \mathbf{r}_L^I}{\partial \alpha_b} \times \frac{\partial \mathbf{r}_L^I}{\partial \tau} \right| = \sqrt{(\alpha_b p_1 r_b \cos \tau)^2 + (\alpha_b p_1 r_b \sin \tau)^2 + (\alpha_b r_b^2)^2} = r_b \alpha_b \sqrt{p_1^2 + r_b^2}$$

$$\begin{cases} n_{x_1 L} = \frac{p_1 \cos \tau}{\sqrt{p_1^2 + r_b^2}} = \sin \gamma \cos \tau \\ n_{y_1 L} = \frac{p_1 \sin \tau}{\sqrt{p_1^2 + r_b^2}} = \sin \gamma \sin \tau \\ n_{z_1 L} = \frac{r_b}{\sqrt{p_1^2 + r_b^2}} = \cos \gamma \end{cases} \quad (2.8)$$

In the formula β_b is the base circle helix lift angle of the involute cylindrical worm. $\tan \gamma = \frac{r_b}{p_1}$. So $\mathbf{n}_L^I = -\sin \gamma \cos \tau \mathbf{i}_1 - \sin \gamma \sin \tau \mathbf{j}_1 + \cos \gamma \mathbf{k}_1$.

Same reason the unit normal vector in the coordinate system S_1 at any point on the right-hand tooth surface of the worm is:

$$\mathbf{n}_R^I = \frac{\frac{\partial \mathbf{r}_R^I}{\partial \alpha_b} \times \frac{\partial \mathbf{r}_R^I}{\partial \theta}}{\left| \frac{\partial \mathbf{r}_R^I}{\partial \alpha_b} \times \frac{\partial \mathbf{r}_R^I}{\partial \theta} \right|} = n_{x_1 R} \mathbf{i}_1 + n_{y_1 R} \mathbf{j}_1 + n_{z_1 R} \mathbf{k}_1$$

In the formula:

$$\begin{cases} \frac{\partial \mathbf{r}_R^I}{\partial \alpha_b} = r_b \alpha_b \sin \tau' \mathbf{i}_1 + r_b \alpha_b \cos \tau' \mathbf{j}_1 + 0 \mathbf{k}_1 \\ \frac{\partial \mathbf{r}_R^I}{\partial \theta} = (-r_b \cos \tau' - r_b \alpha_b \sin \tau') \mathbf{i}_1 + (r_b \sin \tau' - r_b \alpha_b \cos \tau') \mathbf{j}_1 + p_1 \mathbf{k}_1 \end{cases}$$

$$\frac{\partial \mathbf{r}_R^I}{\partial \alpha_b} \times \frac{\partial \mathbf{r}_R^I}{\partial \theta} = \begin{vmatrix} \mathbf{i}_1 & \mathbf{j}_1 & \mathbf{k}_1 \\ \frac{\partial \mathbf{x}_1}{\partial \alpha_b} & \frac{\partial \mathbf{y}_1}{\partial \alpha_b} & \frac{\partial \mathbf{z}_1}{\partial \alpha_b} \\ \frac{\partial \mathbf{x}_1}{\partial \theta} & \frac{\partial \mathbf{y}_1}{\partial \theta} & \frac{\partial \mathbf{z}_1}{\partial \theta} \end{vmatrix} = \alpha_b p_1 r_b \cos \tau' \mathbf{i}_1 - \alpha_b p_1 r_b \sin \tau' \mathbf{j}_1 + \alpha_b r_b^2 \mathbf{k}_1$$

$$\left| \frac{\partial \mathbf{r}_R^I}{\partial \alpha_b} \times \frac{\partial \mathbf{r}_R^I}{\partial \theta} \right| = \sqrt{(\alpha_b p_1 r_b \cos \tau')^2 + (\alpha_b p_1 r_b \sin \tau')^2 + (\alpha_b r_b^2)^2} = r_b \alpha_b \sqrt{p_1^2 + r_b^2}$$

$$\begin{cases} n_{x_1 R} = \frac{p_1 \cos \tau'}{\sqrt{p_1^2 + r_b^2}} = \sin \gamma \cos \tau' \\ n_{y_1 R} = \frac{-p_1 \sin \tau'}{\sqrt{p_1^2 + r_b^2}} = -\sin \gamma \sin \tau' \\ n_{z_1 R} = \frac{-r_b}{\sqrt{p_1^2 + r_b^2}} = \cos \gamma \end{cases} \quad (2.9)$$

In the formula β_b is the base circle helix lift angle of the involute cylindrical worm. $\tan \gamma = \frac{p_1}{r_b}$. So $\mathbf{n}_R^1 = \sin \gamma \cos \tau' \mathbf{i}_1 - \sin \gamma \sin \tau' \mathbf{j}_1 + \cos \gamma \mathbf{k}_1$.

Relative speed of movement at the meshing point of the worm and the tooth surface of the face gear. In the worm-surface gear transmission coordinate system, it can be seen that the worm rotates around the k_w axis at an angular velocity ω_1 , and the surface gear does a rotational motion around the k_f at an angular velocity ω_2 . Then the relative motion speed of the meshing points of the two components in the coordinate system S_w is [19]:

$$\mathbf{v}_w^{12} = [(\boldsymbol{\omega}_w^1 - \boldsymbol{\omega}_w^2) \times \mathbf{r}_w] - (\mathbf{o}_w \mathbf{o}_f \times \boldsymbol{\omega}_w^2)$$

In the formula: $\mathbf{o}_w \mathbf{o}_f$ is the eccentricity between the worm face gears, the direction is pointed from the worm to the face gear, the superscript "1,2" represents the worm and the face gear, respectively, and the w in the subscript indicates that it is in the coordinate system S_w .

$\boldsymbol{\omega}_w^1$ is the angular velocity of rotation of the worm in S_w coordinate system:

$$\boldsymbol{\omega}_w^1 = [0 \ 0 \ \omega_1]^T$$

$\boldsymbol{\omega}_f^2$ is the angular velocity of rotation of the worm in S_f coordinate system:

$$\boldsymbol{\omega}_f^2 = [0 \ 0 \ -\omega_2]^T$$

Due to the S_w coordinate transformation with the S_f coordinate system, the rotational angular velocity of the surface gear in the S_w coordinate system:

$$\boldsymbol{\omega}_w^2 = [0 \ -\omega_2 \ 0]^T$$

Suppose that point M is a common point of the two members of the worm and the surface gear during the meshing process, and the coordinates of the point in the S_1 of the moving coordinate system (x_1, y_1, z_1) , assuming that the vector vector \mathbf{r}_1 is a vector representing the position of point M in the S_1 coordinate system, including:

$$\mathbf{r}_1 = [x_1, y_1, z_1]^T$$

Then the vector \mathbf{r}_w point M in the S_w coordinate system can be regarded as the vector vector \mathbf{r}_1 rotated counterclockwise around the k_w axis φ_1 , and its coordinates can be expressed as:

$$\left. \begin{array}{l} x = x_1 \cos \varphi_1 - y_1 \sin \varphi_1 \\ y = x_1 \sin \varphi_1 + y_1 \cos \varphi_1 \\ z = z_1 \end{array} \right\}$$

Its coefficient matrix can be listed as the following square matrix:

$$\begin{bmatrix} \cos \varphi_1 & -\sin \varphi_1 & 0 \\ \sin \varphi_1 & \cos \varphi_1 & 0 \\ 0 & 0 & 1 \end{bmatrix}$$

Write the above matrix in its general form and denote it by M_{w1}' :

$$M_{w1}' = \begin{bmatrix} a_{11} & a_{12} & a_{13} \\ a_{21} & a_{22} & a_{23} \\ a_{31} & a_{32} & a_{33} \end{bmatrix} = \begin{bmatrix} \cos \varphi_1 & -\sin \varphi_1 & 0 \\ \sin \varphi_1 & \cos \varphi_1 & 0 \\ 0 & 0 & 1 \end{bmatrix}$$

Then the vector \mathbf{r}_1 transformed from a coordinate system S_1 to a coordinate system S_w , there is:

$$\mathbf{r}_w = M_{w1}' \mathbf{r}_1 = \begin{bmatrix} x_1 \cos \varphi_1 - y_1 \sin \varphi_1 \\ x_1 \sin \varphi_1 + y_1 \cos \varphi_1 \\ z_1 \end{bmatrix}$$

Under Coordinate System S_w , $\mathbf{o}_w \mathbf{o}_f = [c - b \ a]^T$

Substitute the equation into the relative velocity of the available meshing point at the S_w of the coordinate system:

$$\mathbf{v}_w^{12} = \begin{bmatrix} \omega_2 z_1 - \omega_1 (x_1 \sin \varphi_1 + y_1 \cos \varphi_1) - a \omega_2 \\ \omega_1 (x_1 \cos \varphi_1 - y_1 \sin \varphi_1) \\ -\omega_2 (x_1 \cos \varphi_1 - y_1 \sin \varphi_1) + c \omega_2 \end{bmatrix}$$

The relative velocity of the meshing point at the coordinate system S_1 is:

$$\boldsymbol{v}_I^{12} = \boldsymbol{M}_{w1} \cdot \boldsymbol{v}_w^{12} = \omega_1 \begin{bmatrix} (z_1 - a) \cdot i_{21} \cos \varphi_1 - 2 \cdot x_1 \sin \varphi_1 \cos \varphi_1 - y_1 (\cos^2 \varphi_1 - \sin^2 \varphi_1) \\ (z_1 - a) \cdot i_{21} \sin \varphi_1 - 2 \cdot y_1 \sin \varphi_1 \cos \varphi_1 - y_1 (\sin^2 \varphi_1 - \cos^2 \varphi_1) \\ -i_{21} \cdot (x_1 \cos \varphi_1 - y_1 \sin \varphi_1) + i_{21} \cdot c \end{bmatrix} \quad (2.10)$$

The relative velocity at the meshing point when the tooth surface Σ_1 on the left side of the worm gear is enveloping the worm gear tooth surface I is:

$$\boldsymbol{v}_{IL}^{12} = \boldsymbol{M}_{w1L} \cdot \boldsymbol{v}_w^{12} = \omega_1 \begin{bmatrix} (z_{1L} - a) \cdot i_{21} \cos \varphi_1 - 2 \cdot x_{1L} \sin \varphi_1 \cos \varphi_1 - y_{1L} (\cos^2 \varphi_1 - \sin^2 \varphi_1) \\ (z_{1L} - a) \cdot i_{21} \sin \varphi_1 - 2 \cdot y_{1L} \sin \varphi_1 \cos \varphi_1 - y_{1L} (\sin^2 \varphi_1 - \cos^2 \varphi_1) \\ -i_{21} \cdot (x_{1L} \cos \varphi_1 - y_{1L} \sin \varphi_1) + i_{21} \cdot c \end{bmatrix} \quad (2.11)$$

The relative velocity at the meshing point when the tooth surface Σ_2 on the right side of the worm gear is enveloping the worm gear tooth surface II is:

$$\boldsymbol{v}_{IR}^{12} = \boldsymbol{M}_{w1R} \cdot \boldsymbol{v}_w^{12} = \omega_1 \begin{bmatrix} (z_{1R} - a) \cdot i_{21} \cos \varphi_1 - 2 \cdot x_{1R} \sin \varphi_1 \cos \varphi_1 - y_{1R} (\cos^2 \varphi_1 - \sin^2 \varphi_1) \\ (z_{1R} - a) \cdot i_{21} \sin \varphi_1 - 2 \cdot y_{1R} \sin \varphi_1 \cos \varphi_1 - y_{1R} (\sin^2 \varphi_1 - \cos^2 \varphi_1) \\ -i_{21} \cdot (x_{1R} \cos \varphi_1 - y_{1R} \sin \varphi_1) + i_{21} \cdot c \end{bmatrix} \quad (2.12)$$

Meshing function and meshing equation. At every moment when the worm gear meshes, as shown in the fig 2.4, the conjugate tooth surfaces Σ_1 and Σ_2 are always in tangential contact, there is always a common section and a common normal vector \boldsymbol{n} at the contact point M , and the relative motion speed of the meshing point during the movement is always perpendicular to the common normal vector \boldsymbol{n} , if the two components neither interfere nor separate from each other in the process of continuous transmission, it is necessary to ensure that the relative motion speed of the two at the tangent point \boldsymbol{v}^{12} must be in the direction of the common tangent, That is, the two tooth surfaces need to meet the meshing equation $\boldsymbol{v}^{12} \cdot \boldsymbol{n} = 0$ at the contact point.

Meshing equation of the tooth surface Σ_1 on the left side of the worm to envelop the tooth surface of the worm gear is:

$$\boldsymbol{v}_{IL}^{12} \cdot \boldsymbol{n}_L^1 = 0 \quad (2.13)$$

Substituting Equation (2.8) and Equation (2.11) into Equation (2.13) yields the meshing function as:

$$\Phi_L = \boldsymbol{v}_{IL}^{12} \cdot \boldsymbol{n}_L^1 = \boldsymbol{v}_{x1L}^{12} \cdot \boldsymbol{n}_{xL}^1 \cdot \boldsymbol{v}_{y1L}^{12} \cdot \boldsymbol{n}_{yL}^1 \cdot \boldsymbol{v}_{z1L}^{12} \cdot \boldsymbol{n}_{zL}^1$$

$$\begin{aligned}
&= \omega_1 \{ \sin \gamma \cdot \cos \tau \cdot [(z_{1L} - a) \cdot i_{21} \cos \varphi_1 - 2 \cdot x_{1L} \sin \varphi_1 \cos \varphi_1 - y_{1L} (\cos^2 \varphi_1 - \sin^2 \varphi_1)] \\
&\quad + \sin \gamma \cdot \sin \tau \cdot [(z_{1L} - a) \cdot i_{21} \sin \varphi_1 - 2 \cdot y_{1L} \sin \varphi_1 \cos \varphi_1 - y_{1L} (\sin^2 \varphi_1 - \cos^2 \varphi_1)] \\
&\quad - \cos \gamma \cdot [i_{21} (x_{1L} \cos \varphi_1 - y_{1L} \sin \varphi_1) - i_{21} \cdot c] \}
\end{aligned} \tag{2.14}$$

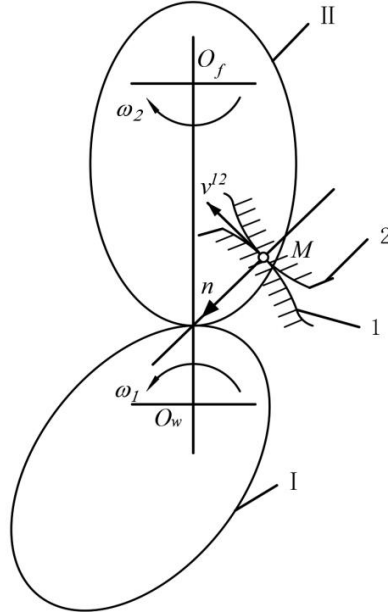


Fig. 2.4. Schematic diagram of worm gear meshing.

Let $\Phi_L = \mathbf{0}$ obtain the meshing equation:

$$\Phi_L = \mathbf{v}_{1L}^{12} \cdot \mathbf{n}_L^1 = \mathbf{v}_{x1L}^{12} \cdot \mathbf{n}_{xL}^1 \cdot \mathbf{v}_{y1L}^{12} \cdot \mathbf{n}_{yL}^1 \cdot \mathbf{v}_{z1L}^{12} \cdot \mathbf{n}_{zL}^1 = \mathbf{0}$$

Meshing equation of the tooth surface Σ_2 on the right side of the worm to envelop the tooth surface of the worm gear is:

$$\mathbf{v}_{1R}^{12} \cdot \mathbf{n}_R^1 = 0 \tag{2.15}$$

Substituting Equation (2.9) and Equation (2.12) into Equation (2.14) yields the meshing function as:

$$\begin{aligned}
\Phi_R &= \mathbf{v}_{1R}^{12} \cdot \mathbf{n}_R^1 = \mathbf{v}_{x1R}^{12} \cdot \mathbf{n}_{xR}^1 \cdot \mathbf{v}_{y1R}^{12} \cdot \mathbf{n}_{yR}^1 \cdot \mathbf{v}_{z1R}^{12} \cdot \mathbf{n}_{zR}^1 \\
&= \omega_1 \{ \sin \gamma \cdot \cos \tau \cdot [(z_{1R} - a) \cdot i_{21} \cos \varphi_1 - 2 \cdot x_{1R} \sin \varphi_1 \cos \varphi_1 - y_{1R} (\cos^2 \varphi_1 - \sin^2 \varphi_1)] \\
&\quad - \sin \gamma \cdot \sin \tau \cdot [(z_{1R} - a) \cdot i_{21} \sin \varphi_1 - 2 \cdot y_{1R} \sin \varphi_1 \cos \varphi_1 - y_{1R} (\sin^2 \varphi_1 - \cos^2 \varphi_1)] \\
&\quad - \cos \gamma \cdot [i_{21} (x_{1R} \cos \varphi_1 - y_{1R} \sin \varphi_1) + c i_{21}] \}
\end{aligned} \tag{2.16}$$

Let $\Phi_R = \mathbf{0}$ obtain the meshing equation:

$$\Phi_R = \mathbf{v}_{1R}^{12} \cdot \mathbf{n}_R^1 = \mathbf{v}_{x1R}^{12} \cdot \mathbf{n}_{xR}^1 \cdot \mathbf{v}_{y1R}^{12} \cdot \mathbf{n}_{yR}^1 \cdot \mathbf{v}_{z1R}^{12} \cdot \mathbf{n}_{zR}^1 = 0$$

Tooth surface equation for offset cylindrical worm drive comprises:
Instantaneous contact line equation; Meshing surface equations.

Instantaneous contact line equation. During the meshing process, the conjugate surfaces Σ_1 and Σ_2 contact each other along a line at each instant, which is called the instantaneous contact line, and in the offset worm drive, the contact line on the tooth surface satisfies both the tooth surface equation and the meshing equation, so it can be obtained:

Contact line equation for the left side of the cylindrical worm cogging (right side of the gear tooth)

$$\begin{cases} \Phi_L = 0 \\ x_{1L} = -r_b \sin \tau + r_b \alpha_b \cos \tau \\ y_{1L} = r_b \cos \tau + r_b \alpha_b \sin \tau \\ z_{1L} = p_1(\tau - \beta_b - \alpha_b) \end{cases} \quad (2.17)$$

Contact line equation for the right side of the cylindrical worm cogging (left side of the gear tooth)

$$\begin{cases} \Phi_R = 0 \\ x_{1R} = r_b \sin \tau' - r_b \alpha_b \cos \tau' \\ y_{1R} = r_b \cos \tau' + r_b \alpha_b \sin \tau' \\ z_{1R} = p_1(\beta_b + \alpha_b - \tau') \end{cases} \quad (2.18)$$

Meshing surface equations. Equation of the meshing surface of Σ_2 on the left side of the worm cog in the S_2

$$\mathbf{r}_{wL} = M_{w1} \mathbf{r}_{1L}$$

Its inter-coordinate conversion matrix M_{w1} is:

$$M_{w1} = \begin{bmatrix} \cos \varphi_1 & \sin \varphi_1 & 0 & 0 \\ -\sin \varphi_1 & \cos \varphi_1 & 0 & 0 \\ 0 & 0 & 1 & 0 \\ 0 & 0 & 0 & 1 \end{bmatrix}$$

The meshing surface equation of Σ_1 on the left side of the worm cog in the S_w can be obtained:

$$\begin{cases} \Phi_L = 0 \\ x_{1L} = -r_b \sin \tau + r_b \alpha_b \cos \tau \\ y_{1L} = r_b \cos \tau + r_b \alpha_b \sin \tau \\ z_{1L} = p_1(\tau - \beta_b - \alpha_b) \\ x_{wL} = x_{1L} \cos \varphi_1 + y_{1L} \sin \varphi_1 \\ y_{wL} = -x_{1L} \sin \varphi_1 + y_{1L} \cos \varphi_1 \\ z_{wL} = z_{1L} \end{cases} \quad (2.19)$$

Similarly, equation of the meshing surface of Σ_2 on the right side of the worm cog in the S_w is:

$$\begin{cases} \Phi_R = 0 \\ x_{1R} = r_b \sin \tau' - r_b \alpha_b \cos \tau' \\ y_{1R} = r_b \cos \tau' + r_b \alpha_b \sin \tau' \\ z_{1R} = p_1(\beta_b + \alpha_b - \tau') \\ x_{wR} = x_{1R} \cos \varphi_1 + y_{1R} \sin \varphi_1 \\ y_{wR} = -x_{1R} \sin \varphi_1 + y_{1R} \cos \varphi_1 \\ z_{wR} = z_{1R} \end{cases} \quad (2.20)$$

Worm gear tooth surface equation. Equation of the meshing surface of Σ_2 on the right side of the face worm gear cog in the S_2 is:

$$\mathbf{r}_{2L} = M_{21} \mathbf{r}_{1L}$$

Its inter-coordinate conversion matrix M_{21} is:

$$\begin{aligned} \mathbf{M}_{2L} &= \mathbf{M}_{2f} \mathbf{M}_{fw''} \mathbf{M}_{w''} \mathbf{M}_w \mathbf{M}_{wI} \\ &= \begin{bmatrix} -\cos \varphi_2 \sin \varphi_1 & \cos \varphi_1 \cos \varphi_2 & \sin \varphi_2 & b \cos \varphi_2 - c \cos \varphi_2 - a \sin \varphi_2 \\ \sin \varphi_1 \sin \varphi_2 & -\cos \varphi_1 \sin \varphi_2 & \cos \varphi_2 & c \cos \varphi_2 - b \sin \varphi_2 - a \sin \varphi_2 \\ \cos \varphi_1 & \sin \varphi_1 & 0 & 0 \\ 0 & 0 & 0 & 1 \end{bmatrix} \end{aligned}$$

The meshing surface equation of Σ_1 on the left side of the worm face gear cog in the S_2 can be obtained:

$$\begin{cases} \Phi_L = 0 \\ x_{1L} = -r_b \sin \tau + r_b \alpha_b \cos \tau \\ y_{1L} = r_b \cos \tau + r_b \alpha_b \sin \tau \\ z_{1L} = p_1(\tau - \beta_b - \alpha_b) \\ x_{2L} = -x_{1L} \cos \varphi_2 \sin \varphi_1 + y_{1L} \cos \varphi_1 \cos \varphi_2 + z_{1L} \sin \varphi_2 + b \cos \varphi_2 - c \cos \varphi_2 - a \sin \varphi_2 \\ y_{2L} = x_{1L} \sin \varphi_1 \sin \varphi_2 - y_{1L} \cos \varphi_1 \sin \varphi_2 + z_{1L} \cos \varphi_2 + c \cos \varphi_2 - b \cos \varphi_2 - a \sin \varphi_2 \\ z_{2L} = x_{1L} \cos \varphi_1 + y_{1L} \sin \varphi_1 \end{cases} \quad (2.21)$$

Similarly, equation of the meshing surface of Σ_2 on the right side of the worm face gear cog in the S_2 is:

$$\begin{cases} \Phi_R = 0 \\ x_{1R} = r_b \sin \tau' - r_b \alpha_b \cos \tau' \\ y_{1R} = r_b \cos \tau' + r_b \alpha_b \sin \tau' \\ z_{1R} = p_1(\beta_b + \alpha_b - \tau') \\ x_{2R} = -x_{1R} \cos \varphi_2 \sin \varphi_1 + y_{1R} \cos \varphi_1 \cos \varphi_2 + z_{1R} \sin \varphi_2 + b \cos \varphi_2 - c \cos \varphi_2 - a \sin \varphi_2 \\ y_{2R} = x_{1R} \sin \varphi_1 \sin \varphi_2 - y_{1R} \cos \varphi_1 \sin \varphi_2 + z_{1R} \cos \varphi_2 + c \cos \varphi_2 - b \cos \varphi_2 - a \sin \varphi_2 \\ z_{2R} = x_{1R} \cos \varphi_1 + y_{1R} \sin \varphi_1 \end{cases} \quad (2.22)$$

2.2 Establishment of 3D model of Offset worm face gear

2.2.1 The condition without root cutting occurs

In the process of enveloping the surface gear, the root cutting phenomenon [20] occurs when the tooth top line of the worm or the tooth top circle of the tool and the theoretical meshing line exceed the pole of the theoretical meshing line (the intersection of the inner common tangent and the base circle).

The speed of the contact point moving with the worm coordinate system \mathbf{v}_w^1 , the speed of movement with the coordinate system of the surface gear \mathbf{v}_w^2 , and the relative speed of the contact between the worm and the tooth surface of the surface gear \mathbf{v}_w^{12}

$$\mathbf{v}_w^2 = \mathbf{v}_w^1 + \mathbf{v}_w^{12} \quad (2.23)$$

When $\mathbf{v}_w^2 = \mathbf{v}_w^1 - \mathbf{v}_w^{12} = \mathbf{0}$, A root cut occurs on the surface gear tooth surface (the root cut point is the sharp point, and the radius of curvature is 0), and there is a root cut boundary line on the tool tooth surface accordingly.

$$\mathbf{v}_{wx}^{12}/\mathbf{v}_{1x} = \mathbf{v}_{wy}^{12}/\mathbf{v}_{1y} = \mathbf{v}_{wz}^{12}/\mathbf{v}_{1z} = -1$$

In the formular:

$$\mathbf{v}_{1x} = \frac{dx_1}{dt} = \frac{\partial x_1}{\partial \alpha_b} \frac{d\alpha_b}{dt} + \frac{\partial x_1}{\partial \tau} \frac{d\tau}{dt} \quad (2.24)$$

$$\mathbf{v}_{1y} = \frac{dy_1}{dt} = \frac{\partial y_1}{\partial \alpha_b} \frac{d\alpha_b}{dt} + \frac{\partial y_1}{\partial \tau} \frac{d\tau}{dt} \quad (2.25)$$

$$\mathbf{v}_{1z} = \frac{dz_1}{dt} = \frac{\partial z_1}{\partial \alpha_b} \frac{d\alpha_b}{dt} + \frac{\partial z_1}{\partial \tau} \frac{d\tau}{dt} \quad (2.26)$$

Considering that the meshing equation $\Phi_R = \mathbf{v}_{1R}^{12} \cdot \mathbf{n}_R^1 = \mathbf{0}$ is an identity for all moments t, there is a derivative for it

$$\frac{\partial\Phi}{\partial\gamma}\frac{d\gamma}{dt} + \frac{\partial\Phi}{\partial\tau}\frac{d\tau}{dt} + \frac{\partial\Phi}{\partial\varphi}\frac{d\varphi}{dt} = 0$$

From $\frac{\mathbf{v}_{wx}^{12}}{\mathbf{v}_{1x}} = \frac{\mathbf{v}_{wy}^{12}}{\mathbf{v}_{1y}} = \frac{\mathbf{v}_{wz}^{12}}{\mathbf{v}_{1z}} = -\mathbf{1}$, there are 3 cases of 2 independent equations,

combined with (2.24)~(2.26), 3 linear equations can be obtained:

$$\begin{cases} \frac{\partial x_1}{\partial \alpha_b} \frac{d\alpha_b}{dt} + \frac{\partial x_1}{\partial \tau} \frac{d\tau}{dt} = -\mathbf{v}_{wx}^{12} \\ \frac{\partial y_1}{\partial \alpha_b} \frac{d\alpha_b}{dt} + \frac{\partial y_1}{\partial \tau} \frac{d\tau}{dt} = -\mathbf{v}_{wy}^{12} \\ \frac{\partial \Phi}{\partial \gamma} \frac{d\gamma}{dt} + \frac{\partial \Phi}{\partial \tau} \frac{d\tau}{dt} = -\frac{\partial \Phi}{\partial \varphi} \frac{d\varphi}{dt} \end{cases} \quad (2.27)$$

$$\begin{cases} \frac{\partial y_1}{\partial \alpha_b} \frac{d\alpha_b}{dt} + \frac{\partial y_1}{\partial \tau} \frac{d\tau}{dt} = -\mathbf{v}_{wy}^{12} \\ \frac{\partial z_1}{\partial \alpha_b} \frac{d\alpha_b}{dt} + \frac{\partial z_1}{\partial \tau} \frac{d\tau}{dt} = -\mathbf{v}_{wz}^{12} \\ \frac{\partial \Phi}{\partial \gamma} \frac{d\gamma}{dt} + \frac{\partial \Phi}{\partial \tau} \frac{d\tau}{dt} = -\frac{\partial \Phi}{\partial \varphi} \frac{d\varphi}{dt} \end{cases} \quad (2.28)$$

$$\begin{cases} \frac{\partial x_1}{\partial \alpha_b} \frac{d\alpha_b}{dt} + \frac{\partial x_1}{\partial \tau} \frac{d\tau}{dt} = -\mathbf{v}_{wx}^{12} \\ \frac{\partial z_1}{\partial \alpha_b} \frac{d\alpha_b}{dt} + \frac{\partial z_1}{\partial \tau} \frac{d\tau}{dt} = -\mathbf{v}_{wz}^{12} \\ \frac{\partial \Phi}{\partial \gamma} \frac{d\gamma}{dt} + \frac{\partial \Phi}{\partial \tau} \frac{d\tau}{dt} = -\frac{\partial \Phi}{\partial \varphi} \frac{d\varphi}{dt} \end{cases} \quad (2.29)$$

It can be known that the equation (2.27) ~ (2.29) is equivalent, one of them can be taken as the research object, such as take equation (2.29), which is about $\frac{d\alpha_b}{dt}$ and $\frac{d\theta}{dt}$ are the system of equations of unknown quantities, then the coefficient matrix K and the augmented matrix G of the system of equations are:

$$K = \begin{bmatrix} \frac{\partial \Phi}{\partial \alpha_b} & \frac{\partial \Phi}{\partial \theta} \\ \frac{\partial x_1}{\partial \alpha_b} & \frac{\partial x_1}{\partial \theta} \\ \frac{\partial z_1}{\partial \alpha_b} & \frac{\partial z_1}{\partial \theta} \end{bmatrix} \quad (2.30)$$

$$\mathbf{G} = \begin{bmatrix} \frac{\partial\Phi}{\partial\alpha_b} & \frac{\partial\Phi}{\partial\theta} & -\frac{\partial\Phi}{\partial\phi} \frac{d\phi}{dt} \\ \frac{\partial x_1}{\partial\alpha_b} & \frac{\partial x_1}{\partial\theta} & -v_{wx}^{12} \\ \frac{\partial z_1}{\partial\alpha_b} & \frac{\partial z_1}{\partial\theta} & -v_{wz}^{12} \end{bmatrix} \quad (2.31)$$

From the equality of the rank of the coefficient matrix \mathbf{K} of the system of equations and the augmented matrix \mathbf{G} , it can be seen that the determinant of the matrix \mathbf{G} is equal to 0, namely:

$$|\mathbf{G}| = \begin{bmatrix} \frac{\partial\Phi}{\partial\alpha_b} & \frac{\partial\Phi}{\partial\theta} & -\frac{\partial\Phi}{\partial\phi} \frac{d\phi}{dt} \\ \frac{\partial x_1}{\partial\alpha_b} & \frac{\partial x_1}{\partial\theta} & -v_{wx}^{12} \\ \frac{\partial z_1}{\partial\alpha_b} & \frac{\partial z_1}{\partial\theta} & -v_{wz}^{12} \end{bmatrix} \quad (2.32)$$

Expand equation (3.30) into the relationship $F(\alpha_b, \theta, \varphi) = 0$, which is connected with the meshing equation $\Phi(\alpha, \theta, \varphi) = 0$, and consider the tooth surface equation of the tool $r_w(\alpha, \theta)$ tooth top line, it can be obtained that the intersection point of the root tangent line on the tooth surface of the tool is the key point where the surface gear tooth surface does not produce root cutting. Therefore, the three parameters α , θ , and φ representing the position of the root cut cut-off point can be obtained by equation (2.33).

$$\left\{ \begin{array}{l} F(\alpha_b, \theta, \varphi) = |\mathbf{G}| = \begin{vmatrix} \frac{\partial\Phi}{\partial\alpha_b} & \frac{\partial\Phi}{\partial\theta} & -\frac{\partial\Phi}{\partial\phi} \frac{d\phi}{dt} \\ \frac{\partial x_1}{\partial\alpha_b} & \frac{\partial x_1}{\partial\theta} & -v_{wx}^{12} \\ \frac{\partial z_1}{\partial\alpha_b} & \frac{\partial z_1}{\partial\theta} & -v_{wz}^{12} \end{vmatrix} = 0 \\ \phi(\alpha_b, \theta) = \arcsin \left(\frac{x_1 \cos(\alpha_b + \beta_b + \theta) \pm y_1 \sin(\alpha_b + \beta_b + \theta)}{\sqrt{a_0^2 + b_0^2}} \right) - \psi \\ \alpha_b = \frac{\sqrt{R_f^2 - R_b^2}}{R_b} \end{array} \right. \quad (2.33)$$

The position parameter of the root cutting critical point $(\alpha_b, \theta, \varphi)$ of the tooth surface of the face gear is brought into the working tooth surface of the face gear the root tangent position coordinates.

The minimum inner radius R_{min} of polygon avoidance root cutting is:

$$R_{min} = \sqrt{x_3^2 + y_3^2} \quad (2.34)$$

2.2.2 The value range of design parameter α_b , β_b and θ

In offset cylindrical worm face gear transmission, the design parameters α_b (involute forming parameter variables), β_b (involute worm end face base circle upper half cogging center angle) and θ (involute spiral surface forming parameter variable) have an important influence on the gear tooth design of worm and surface gears, so before the gear tooth design, the boundary conditions of each design parameter need to be set.

1.The value range of design parameter α_b [21]

As can be seen from fig. 2.2, the design parameters α_b directly determined by the distance rolled by the line MN along the base circle with a radius of r_b , the larger the distance the MN rolls, the greater the corresponding α_b , according to the nature of the involute, the expression of the α_b can be derived from the formula $MN = e\widehat{M} = {}^{\alpha_b}r_b$

$$\alpha_b = \frac{MN}{r_b}$$

In the linear MN, the starting position of N points needs to be determined according to the relationship between the tooth root circle and the base circle, when the radius of the worm tooth root circle r_{f1} less than the radius r_b of the base circle, the starting point of the involute tooth profile formed by the movement of N points is on the base circle, and the value range of the α_b corresponding to the involute is:

$$\alpha_b \in [0, \frac{\sqrt{r_{a1}^2 - r_b^2}}{r_b}] \quad (2.35)$$

When the radius of the worm tooth root circle is greater than the radius of the base circle, the involute tooth profile formed by the N-point movement starts on the tooth root circle, and the value range of the α_b corresponding to the involute tooth profile is:

$$\alpha_b \in [\frac{\sqrt{r_{f1}^2 - r_b^2}}{r_b}, \frac{\sqrt{r_{a1}^2 - r_b^2}}{r_b}] \quad (2.36)$$

2.The value range of design parameter β_b [22]

It can be seen from fig. 2.2 that the parameter β_b is half of the center angle of the base circle corresponding to the cogging thickness on the base circle of the involute worm end face, and from the nature of the involute worm, it can be obtained:

$$t_{p1} = \frac{p_{c1}}{2} = \frac{\pi m}{2}$$

where t_{p1} is the tooth thickness on the involute worm indexing circle; p_{c1} is the tooth pitch on the involute worm indexing circle;

Therefore, the tooth thickness of the base circle of the involute worm t_{b1} as follows:

$$t_{b1} = 2r_b \left[\frac{p_{c1}}{2r_1} + \text{inv}(\alpha_t) \right] = 2r_b \left[\frac{p_{c1}}{2r_1} + \tan \alpha_t - \alpha_t \right] \quad (2.37)$$

From the above equation, we can obtain:

$$\beta_b = \frac{\pi}{z_1} - \frac{t_{b1}}{2r_b} = \frac{\pi}{z_1} - \left[\frac{t_{p1}}{2r_1} + \tan \alpha_t - \alpha_t \right] = \frac{\pi}{2z_1} - \tan \alpha_t + \alpha_t \quad (2.38)$$

3.The value range of design parameter θ [23]

It can be seen from fig. 2.3 that the parameter θ is the parameter variable of the leading involute tooth profile to do spatial spiral motion to form a spiral tooth shape, and the maximum distance $p_1\theta$ along the k_w axis is the tooth width b_1 of the involute worm, so the value range of the original calculation parameter θ is:

$$\theta \in [0, \frac{b_1}{p_1}] \quad (2.39)$$

2.2.3 Involute bias cylindrical worm drive basic geometric parameters

In the analysis of the meshing performance of offset cylindrical worm drive, the ideal initial basic design parameters of worm auxiliary drive are shown in table 2.1.

Table 2.1

Involute bias cylindrical worm drive basic geometric parameters

Parameter name	Symbol	Formula and description
1	2	3
Number of worm teeth	Z_1	6
Number of worm gear teeth	Z_2	30
Worm diameter coefficient	q	14

Ending of table 2.1

1	2	3
Center distance	b	$b = r_1 + h_f$
Number of worm gear teeth	Z_2	30
Worm normal modulus	M_n	$M_t \cos \gamma$
Worm indexing circular helix angle	γ	$\tan \gamma = \frac{Z_1}{q}$
Worm normal pressure angle	α_n	20°
Worm tooth surface working length	B_1	10
Eccentricity	c	7
Ratio	i_{12}	$i_{12} = Z_2/Z_1$
Inner diameter of the worm gear	R_0	11
Face worm gear outer diameter	R_1	15
Tooth top height factor	f	$f = 2 \cos \gamma - 1$
Radial clearance coefficient	c_0	$c_0 = 0.2 \cos \gamma$
Worm end face modulus	M_t	1.5
Worm indexing circle radius	r_1	$r_1 = M_t q / 2(10.5)$
Worm end face pressure angle	α_t	$\tan \alpha_t = \tan \alpha_n / \cos \gamma$
Worm base circle radius	r_b	$r_b = r_1 \cos \alpha_t$
The worm teeth are high	h_a	$h_a = M_t f$
The worm tooth root is high	h_f	$h_f = (f + c_0) M_t$
Worm tooth top circle radius	r_{a1}	$r_{a1} = r_1 + h_a$
Worm tooth root circle radius	r_{f1}	$r_{f1} = r_1 - h_f$

2.2.4 Involute offset cylindrical worm drive three-dimensional modeling

SolidWorks, Pro/E, Catia, and UG are the world's most mature large-scale 3D modeling software using parametric modeling techniques. They are high-performance and powerful engineering automation software packages that can be applied in industrial design, mechanical design, functional simulation, manufacturing, and data management.

With the application of three-dimensional design technology, they have been widely used and recognized in parts design, product assembly, mold development, CNC machining, modeling design, automatic measurement, mechanism simulation, stress analysis, etc. In order to simulate the meshing process of the offset worm and optimize the design and processing, on the basis of the analysis of the offset worm drive, the indirect modeling method is used to simulate the processing process of the offset worm drive on the three-dimensional software. The steps to implement 3D modeling with Solid Works are described below.

Three-dimensional shape of the involute worm

1. Write a program in MATLAB according to formulas (2.5), (2.7), draw the tooth curves of six involute worms that meet the relevant parameter requirements as shown in fig. (4.5), and output the discrete coordinate points on the six involute images to a text file with the suffix .txt.

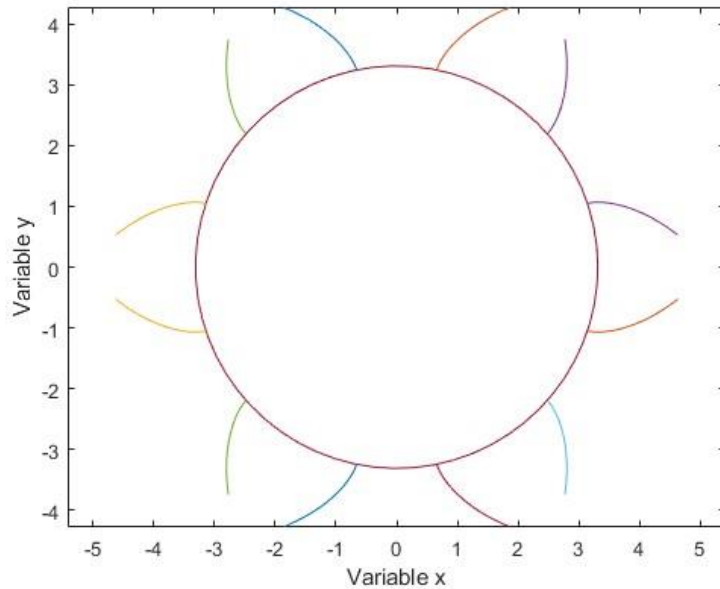


Fig. 2.5. Involute worm teeth.

2. In SolidWorks, the function of creating curves through xyz points is adopted, the specific steps are: insert → curve→ the curve through the xyz points, select the text file containing the discrete coordinate points of the gear teeth, import the data of each point in the involute gear tooth end face tooth diagram into SolidWorks, and the end tooth profile of the involute worm shape can be formed as shown in the fig. 2.6.

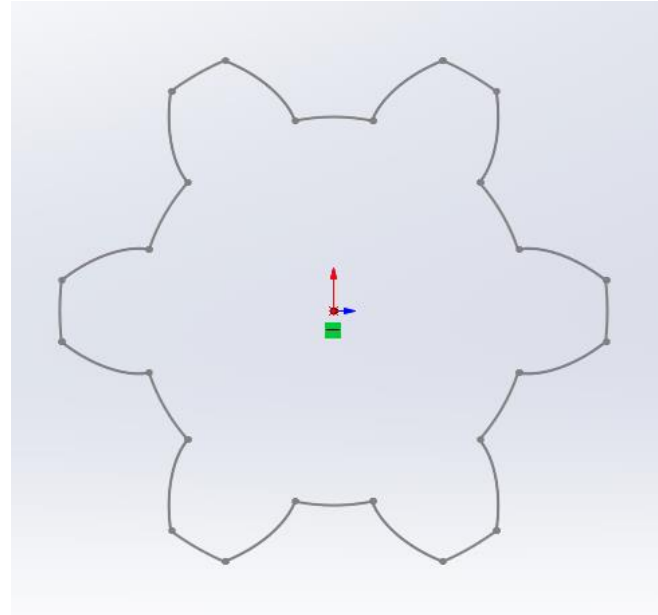


Fig. 2.6. Involute worm section modeling.

3. Using the scan function in SolidWorks, a 3D plot of the involute cylindrical worm can be generated by setting the spiral parameters and scanning the involute end face according to the worm axis as the scan path, as shown in fig. 2.7.

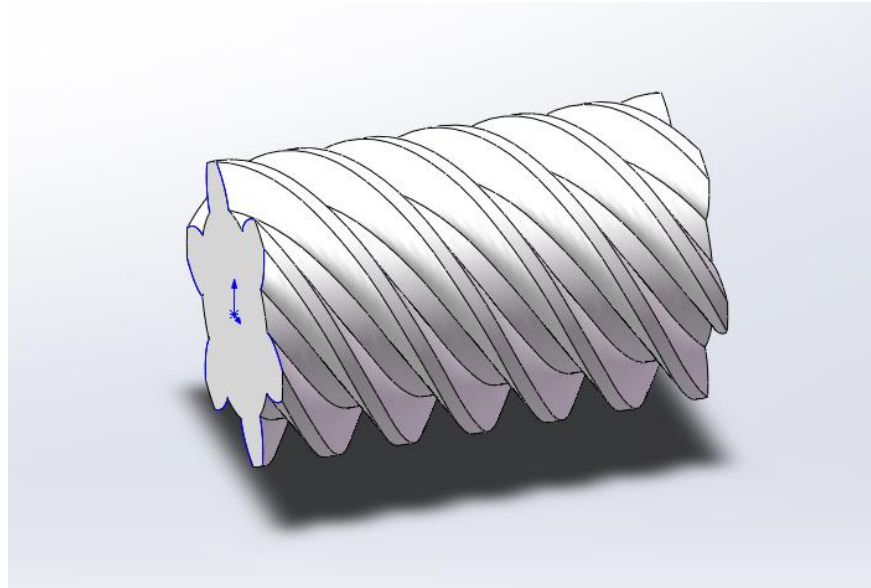


Fig. 2.7. Involute worm 3D model.

Three-dimensional shape of the face gear

Then establish a three-dimensional model of the worm gear, before that, it is necessary to write a program through the tooth surface equation and meshing equation of

the Matlab combined surface gear, the tooth surface is layered in the direction of tooth height, given a series of z values, under each determined z value, and then substituted the initial parameters φ_1 、 φ_2 , the coordinates of a series of discrete points of the surface gear tooth surface can be obtained, and the tooth surface fitted by the discrete points is shown in the figure:

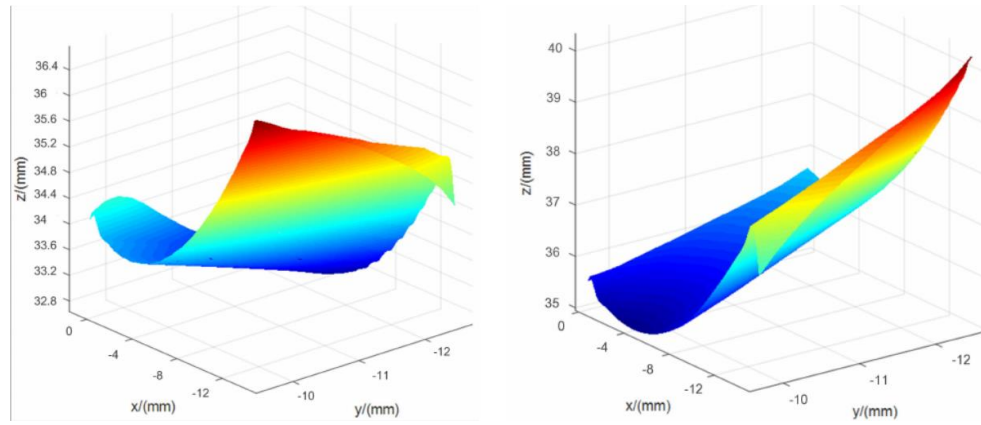


Fig. 2.8. The tooth surface of the worm face gear.

Before generating the tooth surface of the surface gear, the basic parameters of the surface gear must first be determined, that is, the number of teeth, the modulus, pressure angle, etc. The MATLAB programming is then used to calculate the maximum and minimum inner diameters of the face gears, select the appropriate values for the inside and outside diameters at the location of the contact points. From the equations (2.14), (2.16), we can know the equation of the tooth surface of the surface gear gear is an equation with two parameters, α_b and φ_1 .

The generation of flanks can be divided into the following 4 steps:

- (1) Let $Z_2 = c$ (c is constant) give the relationship equation between α_b and φ_1 : $\alpha_b=f(\varphi_1)$.
- (2) According to the meshing conditions, the range of α_b and φ_1 is obtained, and n discrete values are taken for α_b to obtain the correspondence the value of φ_1 .
- (3) Substituting the corresponding values of α_b and φ_1 into the tooth equation of the surface gear can obtain the coordinates of n discrete points, these discrete points fit a curve.

(4) Take different Z_2 values to obtain m curves, and then combine the n curves just now to fit the face teeth the tooth surface of the wheel.

In addition to the working tooth surface, the tooth surface of the face gear also includes the tooth root transition surface, which is formed by the intersection of the cutter's tooth top circle and the tooth profile. The equation form and generation process are similar to the working tooth surface, and can be obtained in the same way. Combining the working tooth surface and the transition surface results in a single-sided tooth of a complete face gear surface. The data point file of the surface gear tooth surface can also be obtained at the same time as the tooth surface. The surface gear tooth surfaces generated in MATLAB are shown in fig. 2.9:

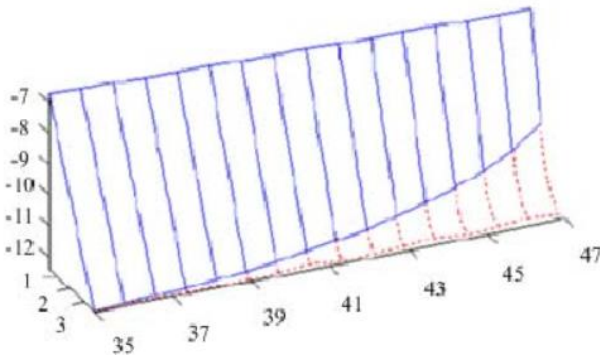


Fig. 2.9. Schematic diagram of the tooth side of the face gear.

The discrete coordinate points of the surface gear flank are calculated in MATLAB and output to a file with the suffix .txt. The calculated discrete coordinate points can form a curve l_i in SolidWorks by insert → curve → through xyz points, then browsing to select the curve file, selecting the default coordinate system, and selecting the desired .txt file, you can get 3 splines through these points. Change the i value to get a different Z_2 value, and use the same method to get other curves. Finally, these curves form the surface gear

A tooth surface of a gear tooth, the specific steps are: insert → surface → boundary surface, and then point by point the formed curve, after clicking and maintaining its default settings, you can get one tooth surface of the face gear, and the other tooth surface can be obtained by the same method. The resulting geometry is shown in fig. 2.8:

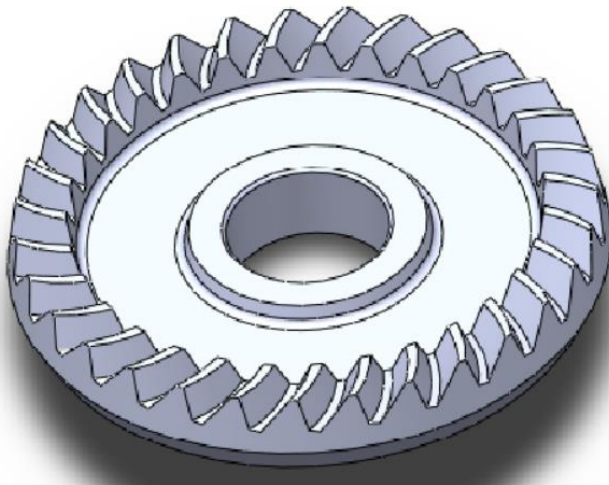


Fig. 2.10. Three-dimensional schematic diagram of face gears.

Conclusion for part 2

Based on differential geometry knowledge and gear meshing principle, the meshing theory of involute bias cylindrical worm drive based on the second quadrant position is derived, the relevant geometric parameters of worm and face gear were determined, and a three-dimensional model of offset worm face gear was established, which lays a foundation for the next analysis of the meshing performance of biased cylindrical worm drive. The main tasks of this chapter are:

1. Taking the third quadrant as the offset position of the worm, the spatial coordinate system of the worm gear is established, and the spatial coordinate transformation matrix of the transformation between the coordinate systems is derived.
2. From the principle of involute formation, the tooth surface equation of the involute cylindrical worm is derived, and then the equation of the common normal vector and the relative motion speed at the instantaneous meshing point of the worm gear meshing process are derived.
3. According to the principle of gear meshing, the contact line equation, meshing equation and tooth surface equation of the worm gear of the worm gear are derived.
4. Determine the inner diameter of the surface gear according to the principle of gear root cutting, and determine the relevant geometric parameters.
5. According to the determined geometric parameters, establish the three-dimensional shape of involute offset cylindrical worm drive.

PART 3. STRENGTH ANALYSIS OF OFFSET WORM FACE GEARS

As gear transmission moves towards high reliability and weight reduction, the design requirements for gears are getting higher and higher. The strength of the face gear directly affects the reliability and weight reduction of the transmission system. At present, the strength check of most gears is considered from two aspects: root bending stress and tooth surface contact stress. The standard calculated surface gear stress values of various gears are significantly higher than the actual stress values, which is more conservative and underestimates the transmission potential of face gears. Therefore, it is necessary to further study and analyze the strength calculation of the surface gear to improve the calculation accuracy.

3.1 Determine the meshing point coordinate value

Regardless of the installation error, calculate the coordinates of the meshing point on the surface gear meshing trajectory, as shown in table 3.1. The meshing points on the gear flank were visualized using MATLAB software, as shown in fig. 3.8. In the simulation, the number of teeth of the tool gear is 6, the module is 1.5 mm , the pressure angle is 20° , the involute worm module is 1.5 mm , the number of teeth is 6, the pressure angle of the indexing circle is the same as that of the tool, the tooth width is 20 mm , the number of teeth of the face gear is 31, and the position parameter L_0 is 230 mm .

Table. 3.1

Offset worm face gear meshing point coordinates without consideration of installation errors

Engagement point	X coordinate	Y coordinate	Z coordinate
1	2	3	4
1	248.08148	2.81990	-57.42583
2	248.13868	3.04436	-57.90010
3	248.18397	3.26759	-58.37272
4	248.26510	3.49552	-58.84870
5	248.31827	3.72000	-59.32100

1	2	3	4
6	248.36518	3.94346	-59.79163
7	248.43991	4.17113	-60.26506
8	248.52626	4.40097	-60.73948
9	248.60230	4.62927	-61.21162
10	248.66980	4.85601	-61.68142
11	248.77909	5.09085	-62.15716
12	248.87140	5.32269	-62.62919

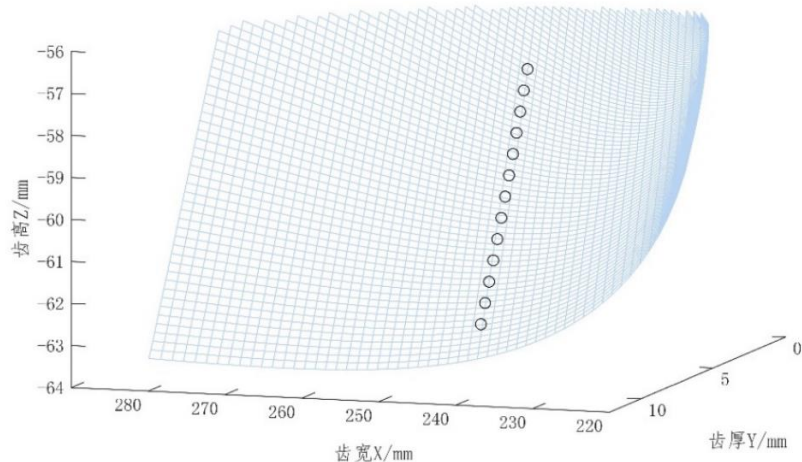


Fig. 3.1. Meshing point on face gear surface.

3.2 Surface gear contact stress calculation

3.2.1 Solve the principal curvature of the surface with the principal direction

According to the knowledge of contact mechanics, the solution process of the contact stress of the worm face gear first needs to obtain the principal curvature of the two surfaces at the meshing point. The coordinate value of the meshing point during the transmission of worm and ace gear has been obtained, and the principal curvature and principal direction at the meshing point need to be calculated before solving the Hertzian contact stress.

Gauss proposed two basic homozymas of surfaces, and it can be seen that the unitary vector representation of surfaces is:

$$n(u, v) = \frac{r_u \times r_v}{|r_u \times r_v|} \quad (3.1)$$

where the first fundamental equation can be obtained from the first fundamental equation, and the first fundamental quantity can be expressed as:

$$E = r_{uu}, F = r_{uv}, G = r_{vv} \quad (3.2)$$

It can be obtained from the second basic homogeneous formula, and the second basic quantity can be expressed as:

$$L = r_{uu} \cdot n, F = r_{uv} \cdot n, G = r_{vv} \cdot n \quad (3.3)$$

In the formula, r_{uu}, r_{uv}, r_{vv} is the second derivative of the tooth surface, the normal curvature K_n of the point on the surface in the direction du/dv is:

$$K_n = \frac{Ldu^2 + 2Mdudv + Ndv^2}{Edu^2 + Fdudv + Gdv^2} \quad (3.4)$$

From the knowledge of differential geometry, the calculation formula of the principal curvature:

$$(EG - F^2)K_n^2 - (EN - 2FN + GL)K_n + (LN - M^2) = 0 \quad (3.5)$$

At non-singularities, the formula for calculating principal curvature must have two different roots of real numbers , i.e. two different principal curvature values at a point on the surface.

According to the knowledge of differential geometry, the characteristic equation [25] for the principal direction is:

$$\left(\frac{dn}{ds} \right) = -k_i g_i$$

The equation that can solve the cardinal direction of the surface is:

$$\begin{cases} K_n(Edu + Edv) - (Ldu + Mdv) = 0 \\ K_n(Fdu + Gdv) - (Mdu + Ndv) = 0 \end{cases} \quad (3.6)$$

Simplification equations can be obtained:

$$(LF - ME) \left(\frac{du}{dv} \right)^2 + (LG - NE) \left(\frac{du}{dv} \right) + (MG - NF) = 0 \quad (3.7)$$

Solving equations (3.7) yields two solutions to du and dv , the two principal directions of the point on the surface.

3.2.2 Hertzian contact stress theory of elastomers

According to the elastic contact theory, it can be seen that points with the same distance between the surfaces of objects will form a set of similar ellipses when they contact in the common tangent plane, which can be expressed in equation (3.8):

$$\begin{cases} z_1 = \rho_{11}x_1^2 + \rho_{12}x_2^2 \\ z_2 = \rho_{21}x_1^2 + \rho_{22}x_2^2 \end{cases} \quad (3.8)$$

In the formula, ρ_{11} , ρ_{12} are the principal curvatures of surface 1, ρ_{21} , ρ_{22} are the principal curvatures of surface 2, equations (3-8) can be expressed in the same coordinate system:

$$H = z_1 - z_2 = Ax^2 + Bx^2$$

In the formula,

$$\begin{cases} A + B = \frac{1}{2}(\rho_{11} + \rho_{12} + \rho_{21} + \rho_{22}) \\ B - A = \frac{1}{2}[(\rho_{11} - \rho_{12})^2 + (\rho_{21} - \rho_{22})^2 + 2(\rho_{11} - \rho_{12})(\rho_{21} - \rho_{22})\cos 2\eta]^{\frac{1}{2}} \end{cases} \quad (3.9)$$

In the formula, η is It is the angle between ρ_{11} and ρ_{21} .

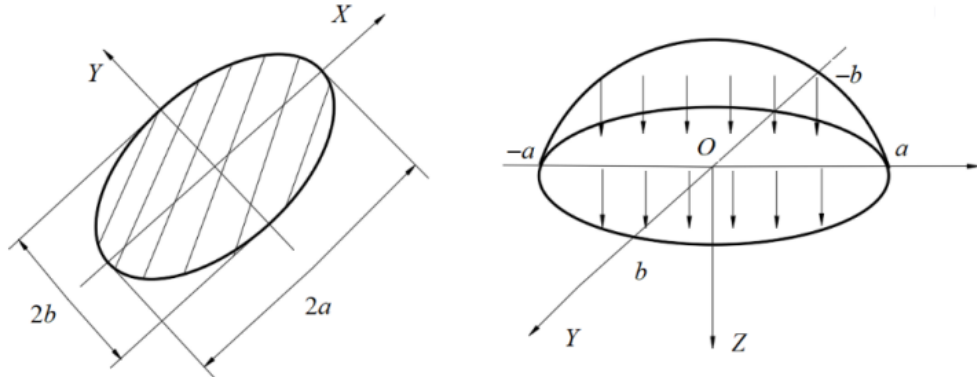


Fig. 3.2. Hertz contact ellipse schematic.

Through the analysis of the load in the elliptic contact area, it can be seen that the deformation at the center of the ellipse is the largest, and the contact stress is also the largest; Moving from the center region to the edge, the corresponding contact stress gradually decreases until the edge position displacement and pressure are zero, as shown in fig. 3.2, so it can be assumed that the load F_n is distributed as a semi-elliptical sphere in the elliptical contact area

$$z = \frac{3F_n}{2\pi ab} \sqrt{1 - \frac{x^2}{a^2} - \frac{y^2}{b^2}}$$

When $x = 0$ and $y = 0$, the maximum contact stress value in the ellipse contact area is:

$$\sigma_{max} = \frac{3F_n}{2\pi ab} \quad (3.10)$$

where a, b are the major and minor semi-axes of the contact ellipse region, which can be solved by:

$$\begin{cases} a = \alpha \left[\frac{3}{4(A+B)} \left(\frac{1-\mu_1^2}{E_1} + \frac{1-\mu_2^2}{E_2} \right) \right]^{\frac{1}{3}} \\ b = \beta \left[\frac{3}{4(A+B)} \left(\frac{1-\mu_1^2}{E_1} + \frac{1-\mu_2^2}{E_2} \right) \right]^{\frac{1}{3}} \end{cases} \quad (3.11)$$

The amount of tooth surface deformation δ in the contact area is:

$$\delta = \gamma \left[\frac{9}{128} (A+B) F_n^2 \left(\frac{1-\mu_1^2}{E_1} + \frac{1-\mu_2^2}{E_2} \right)^2 \right]^{\frac{1}{3}} \quad (3.12)$$

where E_1, E_2, μ_1 , and μ_2 are the elastic modulus and Poisson's ratio of the two-contact material, respectively. α, β, γ are the correlation calculation coefficients, the values of which are determined by $B/A = \cos\theta$, which can be obtained by linear interpolation from table 3.2 [27].

Table 3.2

Table of contact area calculation coefficients

θ	0°	10°	20°	30°	40°	50°	60°	70°	80°	90°
α	∞	6.612	3.778	2.731	2.136	1.611	1.486	1.284	1.128	1
β	0	0.391	0.408	0.493	0.576	0.678	0.717	0.802	0.893	1
γ	—	0.851	1.22	1.453	1.637	1.828	1.875	1.944	1.985	2

3.2.3 Calculation of normal contact force of face gears

Based on Hertzian contact theory, it can be seen that if the surface gear and the involute tooth surface are in contact at the O point, the load torque T is known, the meshing mode between the surface gear and the worm is point contact, and the normal contact force F_n at the meshing point O is collinear with its normal line, as shown in

fig. 3.3, so that its normal contact force is tangent to the base circle, and the normal contact force [24] of the tooth contact point is:

$$F_n = \frac{T}{R_{b1}} \quad (3.13)$$

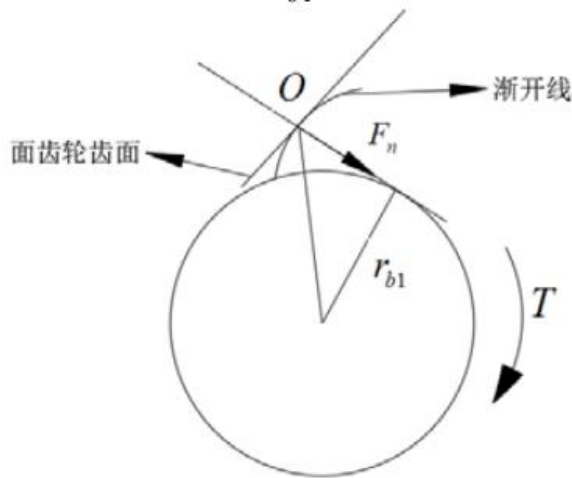


Fig. 3.3. Normal contact force at the meshing point of the face gear.

3.2.4 Surface gear contact stress calculation

According to the calculation method of the hertzian contact stress of worm face gear derived, the calculation process for the calculation of the tooth surface contact stress of worm face gear can be divided into the following steps:

(1) According to equation (3-5) (3-7), calculate the value of the principal curvature of the tooth surface and the main direction of the worm face gear meshing point, and then substitute the principal curvature and the main direction into the equation (3-7) to obtain the values of A and B, and substitute the values of A and B and the gear material coefficient into the equation (3-9) (3-10) to obtain the values of the major semi-axis, the minor semi-axis and the deformation of the contact point of the contact ellipse.

(2) Under the premise of knowing the load T value, the normal contact stress can be calculated from the equation (3-11), F_n and the value is substituted into the equation (3-8) to obtain the maximum contact stress of the tooth surface meshing point of the face gear surface.

(3) The worm and worm face gear take the same material parameters: elastic modulus, $E = 2.07 \times 10^5 N/mm$, Poisson's ratio, $\mu = 0.30$ load torque $T = 30N \cdot m$.

Using the above calculation parameters, the offset surface gear transmission without installation error is calculated, and the calculation result of the worm face gear under the action of the load torque is shown in Table 3-3:

Table 3.3

Calculation results of worm face gear tooth surface contact parameters without installation error

Engagement point	Semi-major axis <i>a</i> (mm)	Semi-minor axis <i>b</i> (mm)	Maximum contact stress σ (Mpa)
1	1.61086	0.13765	1018.40296
2	1.55620	0.14607	993.39532
3	1.51324	0.15373	970.69991
4	1.46679	0.16123	954.87596
5	1.41714	0.16877	944.15833
6	1.36741	0.17619	937.28812
7	1.31680	0.18380	933.01055
8	1.26684	0.19157	930.49110
9	1.21826	0.19953	929.01384
10	1.17149	0.20771	928.02407
11	1.12705	0.21613	927.03205
12	1.08443	0.22494	925.75493

3.3 Finite element calculation of single tooth contact stress of tooth surface gear

3.3.1 Establish a single-tooth finite element model and set boundary conditions

At this stage, the finite element method is more and more widely used in complex mechanical model analysis, a number of commercial software because of its research and development purposes of different use occasions, among which ABAQUS in solving nonlinear problems has the characteristics of good convergence and easy operation, so this paper selects the software to create a bias worm face gear pair single tooth finite element model, counting the offset worm Maximum contact stress at each meshing point of the face gear pair.

Using CATIA, a single-tooth model of involute worm gear and face gear is created, and the meshing positions of the face gear are assembled according to the standard meshing position in the module assembly. Because the gear tooth surface of the worm face is a complex surface, it cannot be reasonably divided into hexahedral meshes in the ABAQUS meshing module. Therefore, the single-tooth contact stress analysis model of the worm face gear is saved as STP forma, imported into the commercial pre-processing software Hyper mesh for hexahedral meshing. Hyper mesh software can ensure the mesh regularization, so that the calculation results are more accurate. The meshed model is then saved in STP format and imported into ABAQUS, as shown in Figure 3.4(a), the contact problem is calculated in ABAQUS, and the 8-node hexahedral linear reduction integration unit (C3D8R) is generally selected, in order to prevent the grid element from being prone to "hourglass" phenomenon in the calculation process, the mesh density needs to be increased.

When setting the boundary condition, a reference point can be established at the center shaft of the worm involute to carry out motion coupling constraints with the inner surface of the worm gear teeth to make the motion of the reference point consistent with the worm gear, and also establish a motion coupling constraint between the face gear and its reference point of the center of rotation. Completely fix the six degrees of freedom of the involute worm and apply the load torque in the direction of the axis at the reference point in the center of the face gear to create a single-tooth finite element model of the offset worm face gear pair, as shown in fig. 3.4(b).

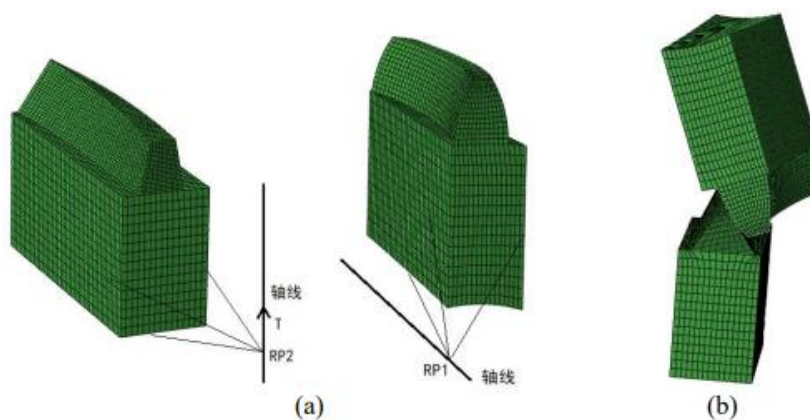


Fig. 3.4. Finite element model of offset worm face gear pair.

3.3.2 Worm face gear finite element calculation results

When calculating the contact stress of each meshing point of the offset worm face gear by the finite element method, the number of finite element meshes is considered to have a greater influence on the calculation accuracy of the contact strength (the denser the mesh, the higher the calculation accuracy, the longer the calculation time, but limited by the performance of the computer itself, selecting a reasonable grid density can reduce costs, etc.). The meshing position 8 in the middle of the offset worm face gear was selected for several precalculations, and when the number of meshes of the finite element model was about 80,000, the error between the finite element calculation result and the analytical calculation result was within 8%, as shown in fig. 3.5.

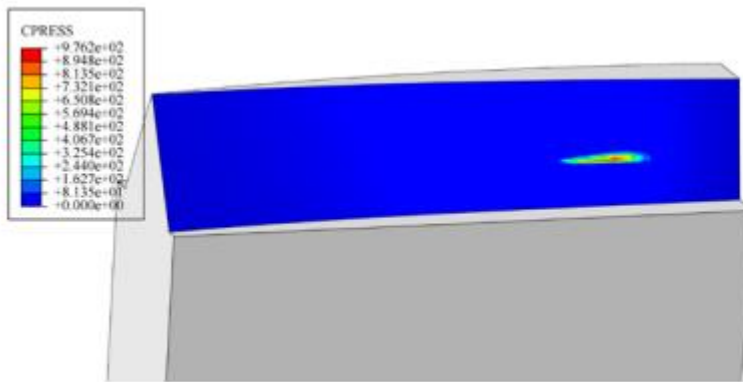


Fig. 3.5. Contact stress cloud at offset worm face gear meshing position 8.

The contact stress of each meshing point obtained by finite element calculation is compared with the contact stress obtained based on the hertzian contact stress method: fig. 3.6 is the contact stress cloud diagram at the position of the meshing point 1 of the face gear, the contact position is close to the tooth top, it is edge contact, and the stress is concentrated at this position, of which the maximum contact stress reaches 1732 MPa, combined with the calculation results of table 3.3, the maximum contact stress of meshing position 1 is much smaller than the value calculated by the finite element method. Moreover, the calculation range of the contact ellipse also exceeds the edge of the tooth surface, resulting in edge contact phenomenon, which does not meet the calculation

conditions of hertzian contact stress, and the value calculated by the analytical method here is unreliable and smaller than the actual contact stress.

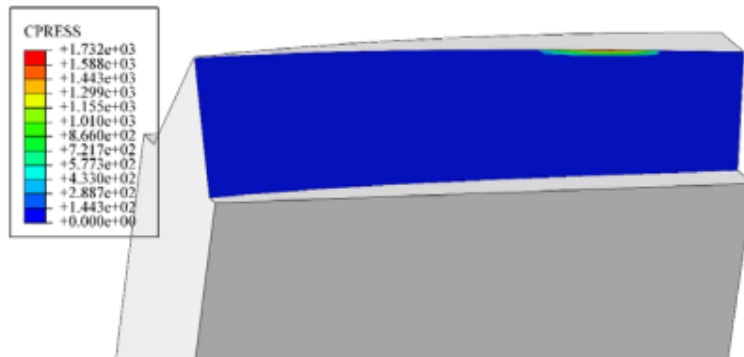


Fig. 3.6. Contact stress cloud at offset worm face gear meshing position 1.

In summary, it can be seen that in the process of worm face gear meshing, edge contact is easy to occur at the top of the tooth, and the calculation results are compared with the analytical method, and the error is large, but without considering the edge contact, the Hertzian contact stress calculation method of a single tooth is not much different from the result obtained by the finite element calculation method, and the error range is within 8%, as shown in Figure 3.7. Since the analysis is for a single tooth to withstand external loads, the contact stress of the worm face gear changes linearly during the meshing transmission.

In the presence of edge contact, the Hertzian contact calculation method does not meet its theoretical assumptions, resulting in a large difference between its calculation result and the finite element solution of the contact stress of the worm face gear, and the calculation results are unreliable.

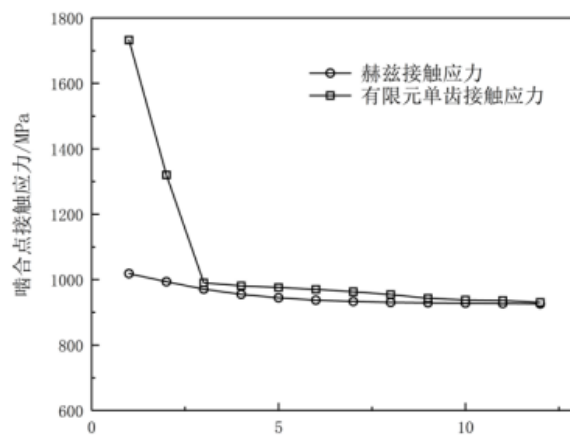


Fig. 3.7. Comparison of two contact stress calculation methods.

3.4 Offset worm face gear loading meshing analysis

Offset worm face gear transmission is different from traditional gear transmission, in the loading and meshing process of offset worm face gear, often produce multiple pairs of gear teeth meshing at the same time, but each pair of gear teeth are subjected to different stresses, which involves the problem of load distribution between gears, which is much more complicated than the single tooth contact stress, so in order to be able to better understand the transmission form of offset worm face gears.

During the multi-tooth loading meshing process of offset worm face gears, material deformation occurs when the tooth surface contact zone is loaded, and the contact point expands into a contact ellipse. In the transmission process, under different working conditions, the contact stress, bending stress, coincidence and transmission error of the surface gear transmission and other performance parameters are also different from the ideal meshing situation of no load. Therefore, it is necessary to perform a loading meshing study on the offset worm face gear.

3.4.1 Basic equations and boundary conditions for the finite element contact of worm face gears

The finite element method has a unique effect on the solution of complex mechanics and physical models, and the multi-tooth loading contact analysis of offset worm face gear is a typical finite element contact problem, and the solution to this problem first requires understanding the basic equations and boundary conditions of mechanics, as well as the contact boundary conditions.

Mechanical equilibrium equations

$$A^i \cdot \sigma^p + f^p = 0 \quad (3.14)$$

where σ^p is the stress vector of the worm and the surface gear, the physical force vector of the worm and the surface gear, and the differential operator (f^p meshing A^i i worm and face gear M , respectively N).

$$A^i = \begin{bmatrix} \frac{\partial}{\partial x_i} & 0 & 0 & \frac{\partial}{\partial y_i} & 0 & \frac{\partial}{\partial z_i} \\ 0 & \frac{\partial}{\partial x_i} & 0 & \frac{\partial}{\partial x_i} & \frac{\partial}{\partial z_i} & 0 \\ 0 & 0 & \frac{\partial}{\partial z_i} & 0 & \frac{\partial}{\partial y_i} & \frac{\partial}{\partial x_i} \end{bmatrix}$$

$$\sigma^p = [\sigma_x \quad \sigma_y \quad \sigma_z \quad \tau_{xy} \quad \tau_{yz} \quad \tau_{zx}]_p^T$$

$$f^p = [f_x \quad f_y \quad f_z]_p$$

(2) Geometric equation of strain displacement relationship

$$\varepsilon_p = L^p \cdot u^p \quad (3.15)$$

where ε_p is the strain vector of worm and face gear, L^p is the differential operator, and u^p is the displacement component of worm and surface gear.

$$L^p = [\varepsilon_x \quad \varepsilon_y \quad \varepsilon_z \quad \gamma_{xy} \quad \gamma_{yz} \quad \gamma_{zx}]_p^T$$

$$u^p = [u_x \quad v_y \quad w_z]_p^T$$

(3) Stress-strain relationship equation

$$\sigma_p = D^p \cdot \varepsilon^P \quad (3.16)$$

where D^p is the elastic matrix, whose value is related to the elastic modulus E and Poisson's ratio μ .

$$D^p = \begin{bmatrix} 0 & \frac{\nu}{1-\nu} & \frac{\nu}{1-\nu} & 0 & 0 & 0 \\ \frac{\nu}{1-\nu} & 1 & \frac{\nu}{1-\nu} & 0 & 0 & 0 \\ \frac{\nu}{1-\nu} & \frac{\nu}{1-\nu} & 1 & 0 & 0 & 0 \\ 0 & 0 & 0 & \frac{1-2\nu}{2(1-\nu)} & 0 & 0 \\ 0 & 0 & 0 & 0 & \frac{1-2\nu}{2(1-\nu)} & 0 \\ 0 & 0 & 0 & 0 & 0 & \frac{1-2\nu}{2(1-\nu)} \end{bmatrix}$$

The equation can only be solved when the stress-strain state in contact between two elastic objects satisfies the above three basic equations as well as the force boundary and the displacement boundary.

(4) Force boundary conditions

$$T^p = n^p \cdot \sigma^p \quad (3.17)$$

where T^p is the T^p surface force on the boundary and n^p is the n^p matrix related to the normal vector outside the boundary.

$$T^p = [T_x \quad T_y \quad T_z]_p^T$$

$$n^p = \begin{bmatrix} n_x & 0 & 0 & n_x & 0 & n_x \\ 0 & n_y & 0 & n_y & n_y & 0 \\ 0 & 0 & n_z & 0 & n_z & n_z \end{bmatrix}$$

(4) Displacement boundary conditions

$$u^p = u^{-p} \quad (3.18)$$

3.4.2 Contact Interface Conditions

Tooth surface contact conditions include: (1) tangential contact conditions (2) normal contact conditions. Among them, the tangential contact judgment condition is whether the two contact tooth surfaces have friction constraints, while the normal contact condition is the condition for determining whether the two tooth surfaces enter the contact, which can be explained by kinematics and dynamics. Since the finite element model calculated in this paper meshes in an ideal state, ignoring the inter-tooth surface friction, only the normal contact conditions need to be considered.

The meshing gear teeth meet the conditions of inaccessibility in kinematics, that is, the worm tooth surface and the surface gear tooth surface N cannot penetrate or interfere during the meshing motion, which can be expressed by mathematical equations as: M

$$g^q = g(x^m, q) = (x^m - x^n) \cdot n^N \quad (3.19)$$

In the formula, the g^q shortest distance between the two tooth surfaces $g^q > 0$ indicates that the two meshing tooth surfaces are in contact; $g^q = 0$ Just contact between the two meshing tooth surfaces; $g^q < 0$ The two meshing tooth surfaces penetrate each other; x^m is the position coordinate vector of a point on the two meshing tooth surfaces; x^n is the point law vector.

When the worm is in contact with the surface gear, the normal contact force generated by the two tooth surfaces is explained from the dynamic conditions as pressure, and its mathematical expression is:

$$F_n^p \leq 0 \quad (3.20)$$

In the formula, the F_n^p normal contact pressure vector of the tooth surface.

3.4.3 Multi-tooth meshing of worm face gears

Both the type of finite element and the meshing technology affect the calculation accuracy of the finite element model, and there are many types of finite element meshing, which can be automatically meshed directly in the meshing module of the finite element software ABAQUS, or you can choose professional pre-processing software for meshing. Since the tooth surfaces on both sides of the worm face gear are convex and concave tooth surfaces, which is too complex and difficult to divide directly in ABAQUS, this paper chooses to use the professional pre-processing software Hyper Mesh to divide the mesh, Hyper Mesh has a strong finite element meshing ability, which can segment the complex finite element model and refine the local mesh, so as to improve the quality of finite element meshing.

Import the model

The modeling process of the surface gear drive model has been described earlier, and the built cylindrical worm and face gear model is imported into ANSYS [33]. Since the gears and cylindrical worms are often not in the assembly position under the default coordinate system of the system during the import process, it is necessary to select different coordinate systems, and then move and rotate to make the cylindrical worm and surface gear in the assembly position. The assembled surface gear transmission model is shown in fig. 3.8.

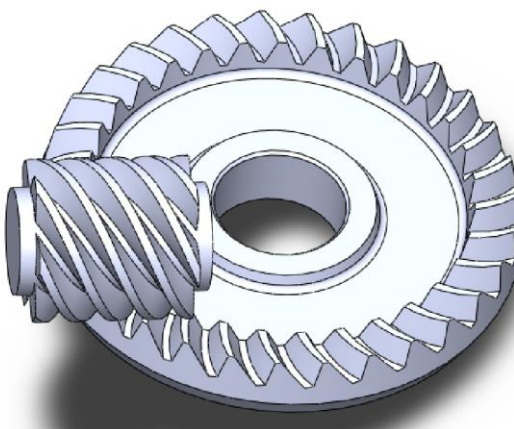


Fig. 3.8. Surface gear drive assembly model.

Set element types and material properties

Solid element type Select *solid45 Cell*. The material was chosen for the commonly used 45-gauge steel. Modulus of elasticity, $112.06 \times 10^9 \text{ Pa}$ material density, 7800 kg/m^3 cypress ratio $\mu = 0.30$. In order to define the contact surfaces of cylindrical and face gears, contact elements must be used and 3D surfaces must be defined *targe170 conta174*. The real constant numbers of the contact surface and the target face must be the same.

Meshing

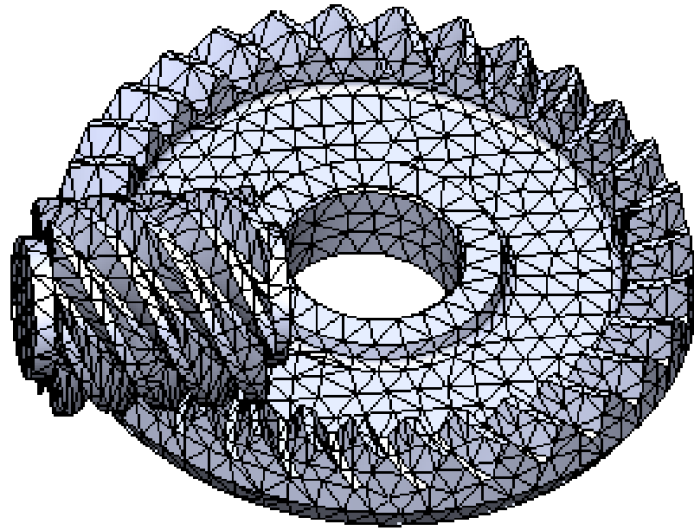


Fig 3.9. Offset worm face gear drive mesh model.

Mesh the opposite gear drive model [34], use ANSYS Main Menu > Preprocessor > Mesh Tool commands, go to Global settings in the Mesh Tool, select the defined element type, the coordinate system where the material number is located, and then divide it with a free grid. The meshed model is shown in Fig. 3.9.

Defining Contact

After meshing is complete, there is no continuity between the face gear and the cylindrical worm, and some form of connection must be established between them. Just as all nodes on the surface of the surface gear contact surface are selected and then a node group is created, the contact surface node of the corresponding cylindrical gear is defined

as another node group. Determine the cell properties to *targe170* and *contac174* then create contact pairs from Main Menu > Preprocessor > Modeling > Create > Contact Pair.

Specify the analysis type to impose constraints

Select the menu Main Menu>Solution>Analysis Type>New AnalysisSelect modal analysis. In Analysis Options, set the subspace option to "ON" and enter 6 in number of modes to extract. Click ok to display the Subspace Modal Analysis window with default settings and click ok. The constraint is that both the face gear and the cylindrical worm have a degree of freedom of rotation around the axis.

3.4.4 Worm face gear strength analysis

This section is calculated according to the settings of 5.1 face gear loading contact analysis pretreatment, in order to find the change law of contact stress and bending stress of worm face gear pair under three different working conditions, and analyze the influence law of different loads on worm face gear.

Contact stress of worm face gear multi-tooth model

Using the ABAQUS post-processing module, the result cloud of the three load loading meshes of the worm face gear can be extracted to visualize the area where the contact stress occurs, as well as the values and positions of the maximum and minimum contact stresses. In this study, the five-tooth model of worm face gear was selected, and the middle teeth of worm and face gear were taken as the research object, and the contact stress changes of intermediate teeth during the whole meshing cycle were analyzed.

Fig. 3.10 shows the contact stress cloud diagram when the worm face gear is $2 \text{ kN} \cdot \text{m}$ loaded. a, b, and c correspond to the contact stress at the top, middle of the tooth and the position of the tooth root (the same below). It can be seen from fig. 3.10 that the contact area between the involute worm and the face gear under this load torque is elliptical, and the contact stress is also distributed according to the ellipse, which is in line with the Hertzian theory of point contact. As the load increases, when the load reaches $6 \text{ kN} \cdot \text{m}$ and $10 \text{ kN} \cdot \text{m}$ the contact stress cloud is shown in fig. 3.10-3.12. The contact area between the involute worm and the surface gear expands, the contact area is elliptical, the maximum contact stress value is located in the center of the ellipse, and the stress value

decreases rapidly at a position away from the center. Edge contact occurs when the contact area is close to the tooth top, where the stress concentration causes the contact stress value to be greater than the normal contact area between the tooth root and the tooth surface. As shown in fig. 3.10, the offset worm face gear tooth top position stress value is 621.6 MPa, the normal contact area stress value is 527.3 MPa, and the tooth root position contact stress value is 294.9 MPa. Fig. 5-5 shows that the biased worm face gear tooth top position stress value is 974.3 MPa, the normal contact area stress value is 822.9 MPa, and the tooth root position contact stress value is 565.6 MPa; fig. 3.12. The offset worm face gear tooth top position stress value is 1356 MPa, the normal contact area stress value is 944.7 MPa, and the tooth root position contact stress value is 762.2 MPa.

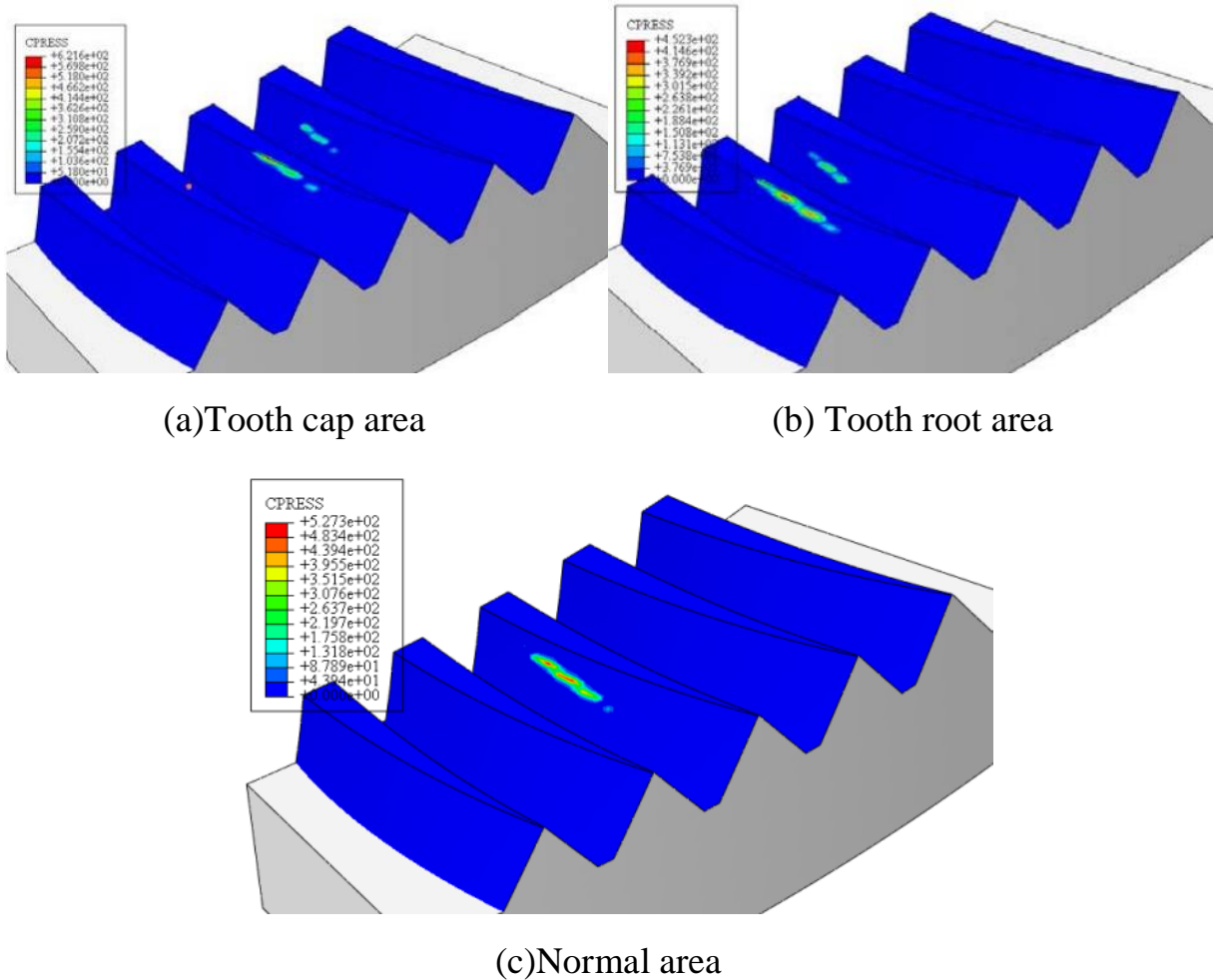


Fig. 3.10. Load of $2 \text{ KN} \cdot \text{m}$ worm face gear contact stress cloud.

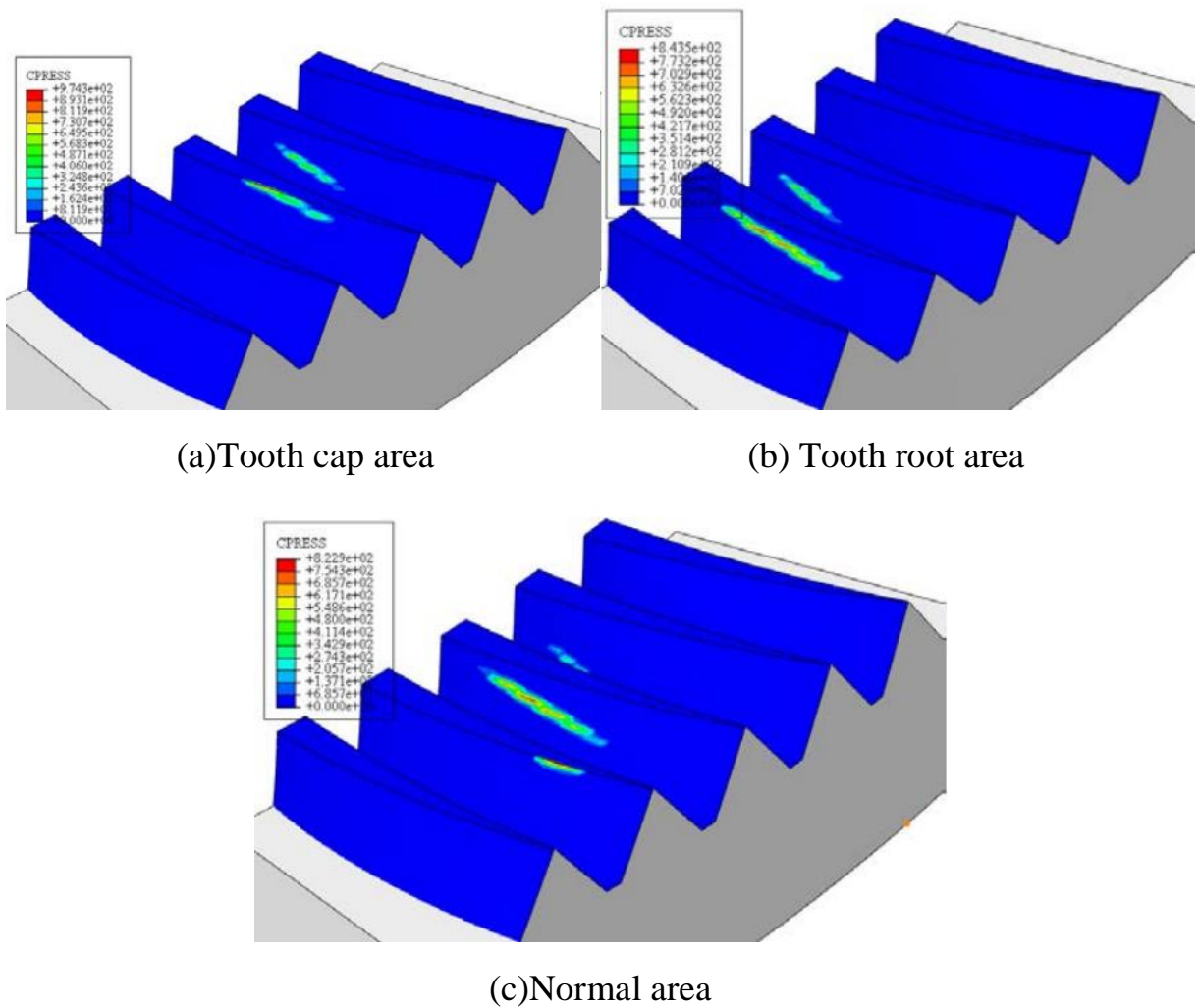
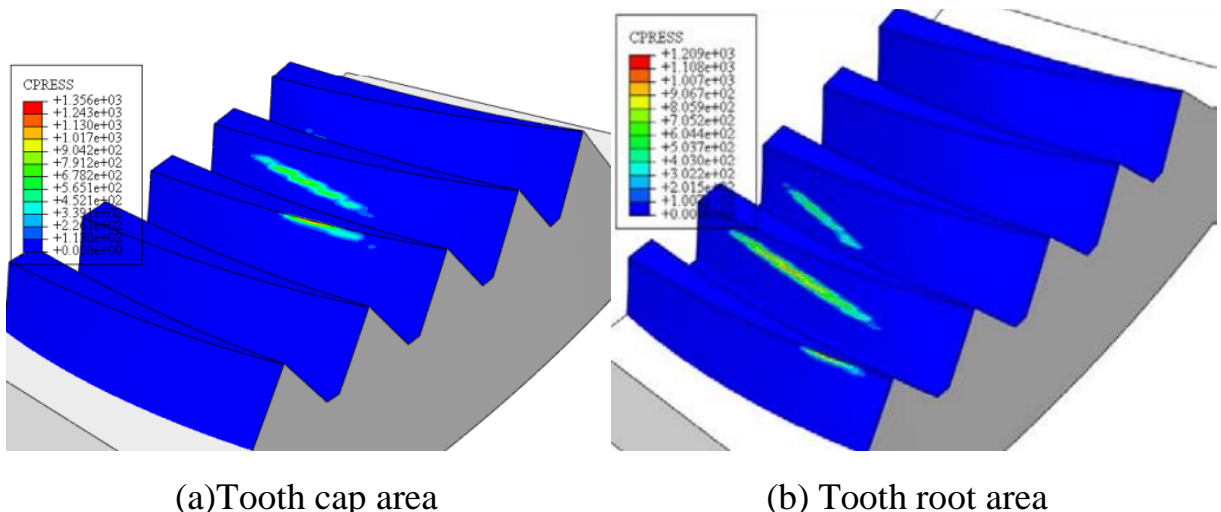
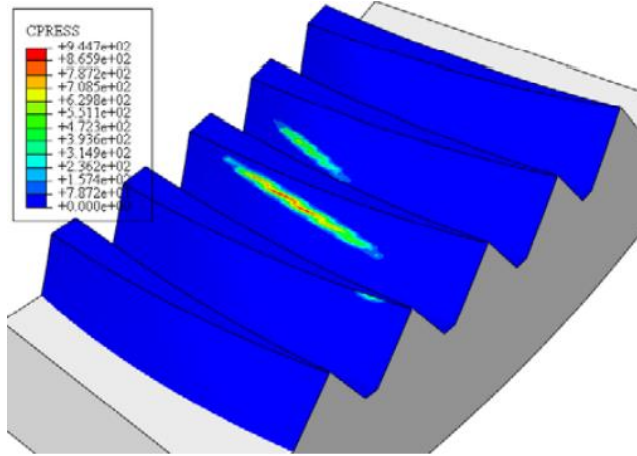


Fig 3.11. Load of $6 \text{ KN} \cdot \text{m}$ worm face gear contact stress cloud.





(c)Normal area

Fig. 3.12. Load of $10 \text{ KN} \cdot \text{m}$ worm face gear contact stress cloud.

By analyzing the above worm face gear contact stress cloud diagram, it can be seen that:

(1) The contact area between the involute worm and the tooth surface of the surface gear is oval and the contact stress of the ellipse center is the largest, and the contact area gradually expands with the increase of the applied load. At the top of the tooth, the meshing area extends to the edge of the tooth surface, and the stress concentration makes the contact stress greater than in other contact positions.

(2) Stress concentration will also occur at the involute worm tooth surface close to the tooth root. In order to make the offset worm face gear pair transmission more stable, it can be practiced in the direction of tooth height or along the tooth width direction to improve the bearing capacity of the face gear pair.

(3) With the increase of the applied load, the coincidence of the face gear increases.

Bending stress of multi-tooth model of offset worm face gear

The bending stress of the gear reflects the fatigue breaking ability of the gear root, which can be regarded as a fatigue strength, so the bending stress cloud of the surface gear can be output in the ABAQUS post-processing module. In the complete meshing cycle of the middle teeth of the worm face gear, the position of the bending stress moves from the outer radial to the inner diameter, and the bending stress at the root of the tooth is the greatest when the face gear is at the highest point of the double tooth meshing. As shown in fig. 3.13, 3.14, 3.15 is the maximum bending stress diagram of the worm face gear

under the action of three loads ($2\text{KN} \cdot \text{m}$, $6\text{ KN} \cdot \text{m}$, $10\text{ KN} \cdot \text{m}$), and the maximum stress values of the face gear are respectively 129MPa , 167MPa , 228MPa .

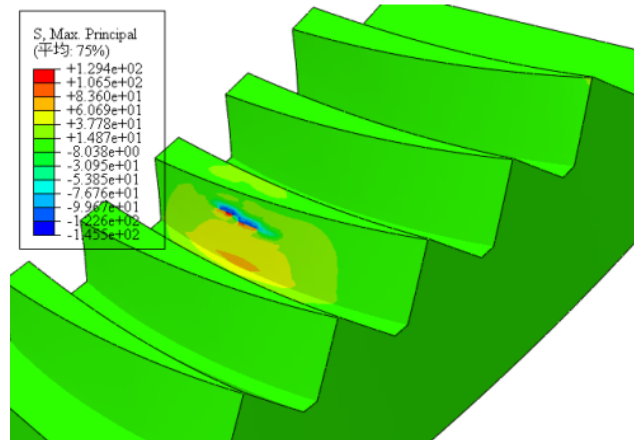


Fig. 3.13. Load $2\text{ KN} \cdot \text{m}$ Maximum bending stress diagram of offset worm face gear pair.

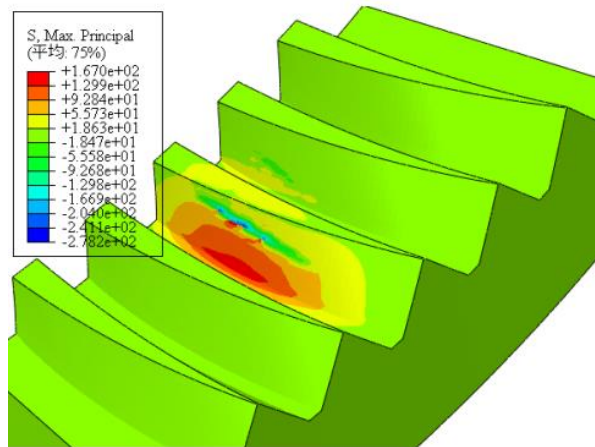


Fig. 3.14. Load $6\text{ KN} \cdot \text{m}$ Maximum bending stress diagram of load worm face gear pair.

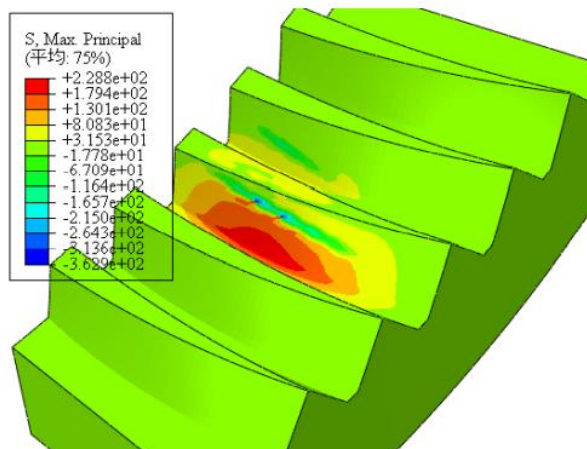


Fig. 3.15. Load $10\text{ KN} \cdot \text{m}$ Maximum bending stress diagram of the face gear pair at load.

Fig. 3.16 shows the bending stress $10 \text{ KN} \cdot \text{m}$ change plot of the worm face gear pair intermediate tooth throughout the meshing cycle under load, recording the bending stress value at each contact position from entering the meshing to exiting the mesh. It can be seen from the figure that the maximum bending stress occurs on the transition surface of the worm face gear. When the worm face gear is located at the highest point of the double-tooth meshing zone, the maximum bending stress of the face gear is 228.8 MPa and the maximum bending stress of the worm is 240.6 MPa.

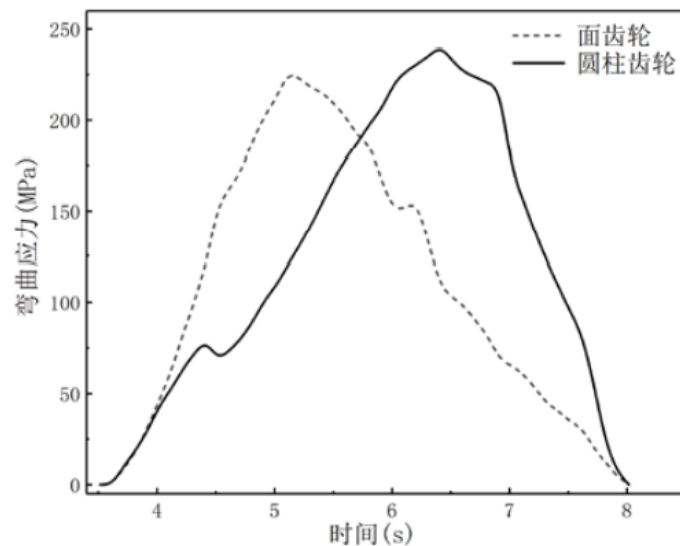


Fig. 3.16. Worm face gear pair bending stress curve.

Conclusion for part 3

On the basis of introducing the principal direction calculation method of the principal curvature of any surface, the principal curvature and principal direction of each meshing point of the gear tooth surface of the offset worm tooth surface are calculated, and the main curvature and principal direction change law of the meshing point when there is no installation error is analyzed.

According to the Hertzian elasticity theory, the contact stress of worm face gear is obtained, and the contact ellipse length, minor semi-shaft and contact stress of each meshing point of worm face gear are calculated.

The finite element method was used to calculate the contact stress of the tooth surface meshing point of the worm face gear, and the calculation accuracy and calculation characteristics of the finite element method and the hertzian analytical method were compared, and it was concluded that in the tooth top contact area, due to the edge contact, the calculation accuracy of the analytical method was worse than that of the finite element method, and the error of the calculation results of the two methods was less than 8% in the middle of the tooth surface.

PART 4. LABOR PROTECTION

Labor protection is to protect the safety and health of workers in the process of production and labor. The state's protection of workers is multifaceted, and the labor protection mentioned here refers specifically to the protection of the safety and health of workers in the process of production and labor. The machinery manufacturing industry provides technical equipment for the entire manufacturing industry and is an important pillar industry of a country. Casting, forging, heat treatment, machining and assembly in the process of machinery manufacturing, these processes have factors that cause health hazards to workers, and the machinery manufacturing industry involves a wide range, the industrial worker team is huge, and the occupational disease hazard factors in the machinery manufacturing industry have an increasingly prominent impact on the health of operators. Therefore, the labor protection of workers in the machinery manufacturing industry is particularly important.

This paper is mainly to study the relevant meshing performance and strength of face gears, therefore, the manufacture of face gears is the basis of this research, in the manufacturing process of face gears, manufacturing workers will face many risk factors at work, next I will list these factors one by one, and formulate relevant protective measures.

4.1 Hazard factors

The main production processes of machinery manufacturing industry include: casting process, forging process, heat treatment process, mechanical processing technology (drilling, milling, boring, turning, planing, grinding, etc.)[28][31], metal surface treatment process, welding and gas cutting process, coating process and assembly.

The main health hazards of the casting process include dust, chemical poisons, noise, vibration, high temperature and heat radiation, high-frequency electromagnetic fields and microwave radiation. Molding sand dust is generated during mold manufacturing, sand falling and cleaning of castings, and metal smoke is generated during pouring. When using resin as an adhesive core, it can contact phenol, formaldehyde and ammonia; Coal furnace operations produce carbon monoxide, carbon dioxide, sulfur dioxide and nitrogen oxides. Noise and vibration are generated in the operation of

mechanical equipment such as vibration and compaction. Sand mold and sand core drying equipment, alloy melting equipment, high temperature and heat radiation are generated during the pouring process. High-frequency electromagnetic fields and microwave radiation are generated when heated in a high-frequency induction furnace or microwave oven.

The main health hazards of the forging process include productive dust, chemical poisons, noise and vibration, high temperature and thermal radiation. Metal dust, coal dust and slag dust can be generated in the process of feeding, furnace and forging in the forging furnace and forging hammer process. Combustion forging furnace can produce carbon monoxide, sulfur dioxide, carbon dioxide, nitrogen oxides and other harmful gases; Magnesium fumes can be produced when magnesium parts. Punching and shearing machines can produce high-intensity noise, generally pulsed noise.

The main health hazards in the heat treatment process include chemical poisons, noise, high temperature and heat radiation, and high-frequency electromagnetic fields. Produced in the process of carburizing, nitriding and other processes, such as the nitriding process produces ammonia, hydride, carbon monoxide, nitrogen oxides. Noise is generated during the operation of mechanical equipment. Various furnaces and heated workpieces generate high temperatures and thermal radiation. High-frequency electric furnaces generate high-frequency electromagnetic fields when they operate.

The main health hazard factor in the metal surface treatment process is chemical poisons. Acid mist, alkali (sulfuric acid, hydrochloric acid, phosphoric acid, sodium hydroxide, nitrogen dioxide, chromate) are usually produced during the process, and some processes use chemicals such as cyanide, nickel compounds, cadmium and its compounds, zinc oxide, chloride, benzene, xylene, ethylene glycol, etc.

The main health hazards in the machining process include dust and noise. Dust is generated during the coarse and fine grinding processes of machining, such as aluminum oxide dust using artificial grinding stones and silicon dust produced by natural grinding stones. Noise is generated when the machine is running.

Welding and gas cutting processes will produce occupational hazards such as ultraviolet rays, welding fumes, manganese and its compounds, ozone, nitrogen oxides, carbon monoxide, and high temperature.

The main health hazard factors in the coating process produce different chemical poisons according to the type and composition of the paint used, such as toluene, xylene, ethyl acetate, butyl acetate, methyl ethyl ketone, methyl isobutyl ketone, etc.

Possible diseases [30]

Diseases caused by dust are mainly pleural mesothelioma caused by silicosis, welder's pneumoconiosis and asbestos. Silicosis can occur in sand turning and sand cleaning operations, and welder pneumoconiosis can occur in electric welding positions.

Diseases caused by physical factors are mainly occupational noise deafness and hand-arm vibration diseases. Noise deafness is common in forging and stamping operators, but in recent years, there have been reports of noise deafness among CNC machine tool operators. Hand arm vibration disease is common in sand cleaning and modeling positions; Occupational diseases caused by chemical poisons mainly include peripheral neuropathy caused by solvent gasoline and methyl n-butyl ketone poisoning, and occupational chronic poisoning caused by benzene compounds.

In addition, acute poisoning can occur. Such as xylene poisoning in boiler manufacturing and canning container manufacturing paint posts; Carbon monoxide poisoning occurred in the pouring post due to poor ventilation and failure of the smelting grate exhaust device; Welding special pipe fittings (zinc) generates metal fumes.

The investigation found that although some workshops have adopted comprehensive ventilation, due to the lack of local ventilation and purification treatment devices, welding fumes, manganese and their compounds still exceed the standard. Some workshops have exceeded the standard of xylene, cyclohexanone and other chemical poisons due to the high position of mechanical ventilation, the density and purification treatment of harmful substances, and the unreasonable organization of the airflow of mechanical ventilation. Some workshops do not adopt local ventilation and dust removal facilities due to manual sand falling and manual sand cleaning, resulting in excessive silica dust. The noise exceeds the standard, mainly because the noise intensity generated by the cutting fluid

being dried with an air gun in the machining post is too large, and it is used frequently, and no sound insulation and muffling devices are adopted.

4.2 Prevention and Control Measures

Silicon dust in casting, organic solvents used in painting workshops, welding fumes in welding workshops, and noise in machining and forging workshops are the main occupational disease hazards in the machinery industry and the key control points of occupational disease hazards in machinery manufacturing projects. To prevent and control occupational hazards in the machinery manufacturing industry, the workshop layout should first be reasonable to reduce the cross-contamination of occupational disease hazards. For example, the melting furnace in the casting process should be placed outdoors or away from public places where people are concentrated; Riveter, electric welding, (painting) painting processes should be arranged separately[29][32].

For the treatment of foundry silica dust, try to use low free silica molding sand, and reduce manual molding and sand cleaning operations. Automatic and closed isolation operations are adopted on sand falling and sand cleaning. Sand cleaning is the position with the highest dust concentration in casting, and should be protected with key points, such as installing a high-power ventilation and dust removal system. Spray wet operation is carried out to prevent secondary dust.

For the treatment of organic solvent hazards, priority should be given to automated, closed equipment or production lines, such as CNC machine tools instead of ordinary machine tools, using robot painting. Coating should try to use low-toxicity organic solvents, with toluene, xylene, ethyl acetate, butyl acetate, methyl ethyl ketone, methyl isobutyl ketone, etc. instead of highly toxic benzene. The coating process adopts the ventilation method of upper and lower rows, the wind speed at the operator's working position is not less than 0.8 m/s, and the painting operation position in the painting booth is equipped with a water curtain (water curtain), anti-poison and detoxification device and washing facilities.

The control of welding fumes hazards focuses on the sealing and automation of production equipment or production lines. For electric welding posts that exceed the

standard, mobile welding fume dust collectors can be designed and equipped with dust removal arms. The dust removal arm is small in size and has high filtration efficiency. For the welding process, a layered air supply treatment scheme can be adopted. In the layered air supply system, air is supplied at low speed in the lower part of the plant, fresh air is directly sent to the work area, and a light and efficient ventilation and purification device is adopted at the operation point.

Noise is one of the important occupational hazards in the machinery manufacturing industry. Noise control mainly includes the treatment of high-intensity noise equipment such as air hammer, air compressor in casting, forging, grinding, polishing, stamping, shearing and cutting in machining. To optimize the process operation flow, such as welding instead of riveting, hydraulic instead of stamping, shot blasting machine adopts automatic and isolated operation. High-intensity noise sources can be centrally arranged, and sound insulation shielding can be set. Aerodynamic noise sources should be silenced at the intake or exhaust ports. The centralized control room and post operation room should be treated with sound insulation and sound absorption. Noise-resistant earplugs or earmuffs should be worn when entering workplaces with noise levels above 85dB(A).

It is also important to take good **measures for poison prevention and emergency rescue**. For workplaces that produce highly toxic gases such as carbon monoxide, hydrogen cyanide, formaldehyde and benzene, such as some special quenching, painting and adhesive positions, emergency rescue plans for acute occupational poisoning accidents should be formulated, warning signs should be set up, and gas masks or respirators should be equipped.

Finally, employees should strengthen personal protection, wear personal protective equipment that meets national standards, and enterprises should attach importance to occupational health management and carry out occupational health inspection, education and training.

The control of welding fumes hazards focuses on the sealing and automation of production equipment or production lines. For electric welding posts that exceed the standard, mobile welding fume dust collectors can be designed and equipped with dust removal arms. The dust removal arm is small in size and has high filtration efficiency. For

the welding process, a layered air supply treatment scheme can be adopted. In the layered air supply system, air is supplied at low speed in the lower part of the plant, fresh air is directly sent to the work area, and a light and efficient ventilation and purification device is adopted at the operation point.

4.3 Fire safety rules for work areas

4.3.1 Fire safety education and training system

1. Every year, we set up fire knowledge bulletin boards, carry out knowledge competitions and other forms to improve the fire safety awareness of all employees.
2. Regularly organize employees to learn fire regulations and various rules and regulations, so as to manage fire according to law.
3. All departments should carry out fire safety education and training according to the characteristics of the post.
4. On-site demonstration and training should be conducted for personnel who maintain and use fire protection facilities.
5. Conduct pre-job fire training for new employees, and can only take up their posts after passing the examination.
6. Employees must undergo re-education and training before changing jobs due to work needs.
7. Special positions such as the elimination control center should be professionally trained, passed the examination, and held a certificate.

4.3.2 Fire prevention inspection and inspection system

1. Implement the level-by-level fire safety responsibility system and post fire safety responsibility system, and implement the patrol inspection system.
2. The fire protection work centralized management functional department conducts fire prevention inspections on the company every day. Conduct a fire inspection of the unit once a month and review the tracking improvement.

3. If a fire hazard is found during the inspection, the inspector shall fill in the fire prevention inspection record and require the relevant personnel to sign the record in accordance with the regulations.

4. The inspection department shall notify the inspected department in time of the inspection situation, and the person in charge of each department shall notify the fire safety inspection every day, and if it is found that there is a fire hazard in the unit, it shall be rectified in time.

5. If the fire hazards found in the inspection are not rectified in time within the specified time, punishment shall be given according to the reward and punishment system.

4.3.3 Management system for safe evacuation facilities

1. The unit shall keep the evacuation channel and safety exit open, and it is strictly forbidden to occupy the evacuation channel, and it is strictly forbidden to install barriers such as fences on the safety exit or evacuation channel that affect the evacuation.

2. Fire safety evacuation instruction signs and emergency lighting facilities that comply with national regulations should be set up according to the specifications.

3. Fire doors, fire safety evacuation instruction signs, emergency lighting, mechanical smoke and air supply, fire accident broadcasting and other facilities should be kept in normal condition, and regular inspection, testing, maintenance and maintenance should be organized.

4. It is strictly forbidden to lock the safety exit during business or work.

5. It is strictly forbidden to close, cover or cover the safety evacuation instruction signs during business or work.

4.3.4 Fire control center management system

1. Familiar with and master the performance of various fire protection facilities to ensure orderly, accurate and rapid operation in the process of fire fighting.

2. Do a good job in fire duty records and shift handover records, and handle fire alarm calls.

3. Handover shifts on time, and do a good job in handing over duty records, equipment conditions, accident handling, etc. Without the procedures for handing over shifts, the personnel on duty shall not leave their posts without authorization.

4. When equipment failure is found, it should be reported in time and notified to the relevant departments to repair it in time.

5. Non-work needs, shall not use the internal telephone of the elimination control center, and non-fire control center duty personnel are prohibited from entering the duty room.

6. It is not allowed to smoke, sleep, read books and newspapers in the elimination control center during working hours, and the handover procedures should be done when leaving the post.

7. When a fire is found, it shall be promptly dealt with urgently according to the fire extinguishing operation plan, and call 119 to notify the public security and fire department and report to the department supervisor.

4.3.5 Maintenance and management system for fire protection facilities and equipment

1. The daily use management of fire protection facilities is the responsibility of full-time administrators, who check the use status of fire protection facilities every day to keep the facilities clean, hygienic and intact.

2. The maintenance and regular technical testing of the technical performance of fire protection facilities and fire fighting equipment shall be the responsibility of the fire protection work management department, and a full-time administrator shall check and understand the operation of fire fighting equipment on time every day. Check the operation records, listen to the opinions of the personnel on duty, arrange maintenance in time if abnormalities are found, and keep the equipment in good technical condition.

3. Regular testing of fire protection facilities and fire fighting equipment:

(1) The test of smoke and temperature sensing alarm system shall be organized and implemented by the fire protection work focal point management department, and the

security department shall participate, and each smoke and temperature sensor probe shall be tested in rotation at least once a year.

(2) Fire pump, sprinkler pump and water curtain pump are opened once a month to check whether it is complete and easy to use.

(3) The positive pressure air supply and anti-smoke exhaust system are tested once every six months.

(4) Indoor fire hydrant and sprinkler drainage test once a quarter.

(5) The test of other fire fighting equipment is determined according to different situations.

4. Fire equipment management:

(1) Regularly check and change the dressing of fire extinguishers twice a year during the winter and summer defense periods.

(2) Send special personnel to manage, regularly inspect fire fighting equipment, and ensure that it is in good condition.

(3) The fire fighting equipment should be inspected frequently, and if it is found to be lost or damaged, it should be immediately replenished and reported to the leader.

(4) The fire fighting equipment of each department shall be managed by the department and designated to be responsible.

4.3.6 Fire hazard rectification system

1. All departments shall eliminate the existing fire hazards in a timely manner.

2. In the fire safety inspection, the fire hazards found should be registered item by item, and the hidden dangers should be sent in writing to each department for rectification within a time limit, and the hidden danger rectification situation should be recorded at the same time.

3. Before the fire hazard is eliminated, each department shall implement preventive measures to ensure fire safety during the rectification period of the hidden danger, and shall propose solutions to major fire hazards that are really unable to be solved, and report to the person responsible for fire safety of the unit in a timely manner, and report to the competent department at the higher level of the unit or the local government.

4. For the fire hazards ordered by the public security fire and rescue department to be corrected within a specified period of time, they shall be corrected within the specified time limit and a reply letter for rectification of the hidden dangers shall be written and reported to the public security fire and rescue department.

4.3.7 Safety management system for fire and electricity use

1. Electricity safety management:

(1) It is strictly forbidden to pull wires at will, and it is strictly forbidden to overload electricity.

(2) The installation of electrical circuits and equipment shall be the responsibility of licensed electricians.

(3) After each department is off work, the power supply that should be turned off should be turned off.

(4) Private use of electric heating rods, electric furnaces and other high-power electrical appliances is prohibited.

2. Fire safety management:

(1) Strictly implement the fire examination and approval system, and when it is really necessary to start hot work, the operating unit shall apply for a "fire permit" to the fire protection work subordinate management department according to the regulations.

(2) Before the hot operation, the flammable and explosive dangerous goods within 5 meters near the fire point should be removed or appropriate safety isolation should be made, and the appropriate type and quantity of fire extinguishing equipment should be borrowed from the security department for standby at any time, and should be returned immediately after the end of the operation, and if there is use, it should be truthfully reported.

(3) If the on-site construction starts at the operation point, it shall apply to the supervisor at or above the manager level (including) of the unit where the operation point is located according to the regulations, and the application department shall send personnel to supervise the site and send personnel to inspect from time to time. Overhead fire

operations more than 2 meters above the ground must ensure that a person below is responsible for extinguishing sparks that may ignite other items at any time.

(4) Those who do not apply for a "fire permit" and work without authorization shall be punished by the personnel of the unit with a minor record and dismissed if serious.

Conclusion of part 4

This chapter introduces the hazards that may occur in the process of processing surface gears, lists the diseases caused by various factors, proposes relevant prevention and control measures, and finally describes the relevant content of fire safety and fire safety.

PART 5. ENVIRONMENT PROTECTION

In the equipment manufacturing industry, the machinery manufacturing industry occupies a major position. In the process of mechanical manufacturing, metal machining is an important process, which can produce many environmental pollution factors. We all realize that environmental protection can not only be carried out at the end of treatment, but also focus on early prevention. In order to reduce the emission of pollutants in the process of metal machining, technical solutions for pollution prevention and waste recycling are discussed.

5.1 Environmental impact of metal machining processes

The cutting process in the metal machining process produces a lot of contaminants, the main of which are chips and cutting fluids. Chips are mainly forming chips and dust chips, forming chips account for a larger proportion, the larger the amount generated in processing, the more serious the waste of resources and the more energy consumption [35]. Moreover, the waste of cutting fluid accelerates tool wear, which is not good for the ecological environment. Dust chips (including tool wear dust) are harmful to operators on the processing site, and can cause diseases and chronic poisoning of the human respiratory system. In the traditional cutting process, it is also necessary to use a large amount of metalworking fluid pouring in the cutting area to play the role of cooling, lubrication, cleaning, chip removal, rust prevention and so on. With the high concern of society to environmental protection, its impact is mainly manifested in:

(1) increased manufacturing costs. In the automotive industry, the cost of metalworking fluids accounts for 16.9% of the total manufacturing costs, including the cost of purchasing cutting fluids, equipment required for the use of metalworking fluids, maintenance and waste liquid disposal costs, etc., while tool costs account for only 7.5% of total manufacturing costs.

(2) Contains mineral oil and sulfur, phosphorus, chlorine and other environmentally harmful additives, if not treated or improperly treated before discharge, will cause pollution to the environment. Usually discharged from untreated cutting fluid, the ordinary oxygen consumption is as high as 20000 mg/L, the chemical oxygen consumption (COD)

is as high as 18000mg/L, and the biological oxygen demand (BOD) is as high as 9300mg/L. In addition, it also contains a large number of buffer etching agents such as sodium nitrite and triethanolamine and surfactants.

(3) Contains harmful ingredients (such as sulfur, nitrite amines, formaldehyde, phenol substances), which are directly in contact with the human body during use, which will induce a variety of skin diseases; The smoke formed by heat volatilization can cause many diseases in the respiratory tract and lungs of workers. After the parts machining process, parts cleaning is generally carried out, and the parts cleaning liquid generally uses PA30-QL degreaser and PA80-3 solid passivator. According to the number of cleaning parts, add a certain amount of cleaning agent and rust inhibitor every 1~2d, and replace the bath every 2 weeks, so that a large amount of parts cleaning liquid is used in the parts cleaning process, which will cause pollution to the environment when discharged.

5.2 Pollution to the environment caused by metal machining process

The process of metal machining process will have cutting processing and other processes, which will appear many pollutants, mainly including chips and cutting fluid, chips include forming and dust two kinds of chips, mostly forming chips, the more it is generated during the processing process, the more resources are wasted, which will also waste cutting fluid, tool wear is accelerated, which is not conducive to the ecological environment. The dust chips will also harm the operator, which is easy to cause human respiratory diseases or chronic poisoning. In the process of traditional cutting, mineral oil, sulfur, phosphorus and other additives that cause pollution to the environment are applied, and if not properly treated, it will harm the environment. In the parts machining process, the parts need to be cleaned, which requires the use of a large amount of cleaning fluid, which will pollute the environment when discharged [36].

5.3 Specific countermeasures to prevent pollution in the metal machining process

5.3.1 Treatment of metalworking fluids

In the machining and cutting, a large number of metalworking fluids will be used, mainly to achieve lubrication, cooling, chip removal, rust prevention and other functions,

so in the process of purchasing metalworking fluids as far as possible to choose practical, complete series of processing media, such as water-soluble, oily, cleaning agents, etc., in order to process the early machine Environmental pollution prevention on auxiliary materials for the process. Filtration and separation purification can be selected to treat the metalworking fluid, which can effectively destroy the stability of the emulsion in the waste liquid, and will use oil for separation, which can be recycled and reused; You can also choose the spray cooling method, mainly to spray the cutting oil to the cutting edge, without a large number of applications of cutting oil can improve the working environment but also improve the service life of the tool.

5.3.2 Treatment of noise and vibration

In the machining of the inevitable noise, vibration and other situations, is also an environmental pollution problem, so in the prevention of the implementation of effective measures in this aspect can not be ignored, in the processing as far as possible to choose the necessary seismic isolation, sound reduction, sound absorption and other measures or placement devices, from equipment to the process are taken appropriate measures, to avoid too much impact, reduce the occurrence of vibration, noise.

5.3.3 Change the traditional machining process

Dry cutting technology[38]. The cost of coolant in the process of use generally includes the cost of use, the cost of purchase, the cost of management, the cost of workpiece cleaning, the separation cost of iron filings and dirty oil, and the disposal of waste liquid Root. Volk Swagen of Germany reported in a statistical analysis that the cost of their coolant use even exceeds the cost of tools and their maintenance. In addition, the use of coolant is also the main source of ecological and workshop environmental pollution of cutting plants and operators' health injuries, with the continuous enhancement of people's awareness of environmental protection and the increasingly strict relevant regulations, reducing or even eliminating the use of coolant has become an inevitable trend. At present, the new dry cutting technology has become a hot spot in green processing technology, and new quasi-dry cutting processes such as micro-lubricated

cutting and cold air cutting have appeared. The dry cutting advocated at present is not simply to remove the coolant in the original process to reduce cutting efficiency, but to carry out the heavy transformation of the traditional cutting process to provide a clean, safe and efficient new process for the new century. In foreign gear processing machine tools, dry rolling cutting technology has been relatively perfected, typical products are Nikki MHI's GE 150A series gear hobbing machine, Germany Liebherr (Liebherr) LC18. Series gear hobbing machine, Gleason 210 H series gear hobbing machine of Gleason company in the United States can cut up to 5 times of traditional machining, and the production efficiency can be increased by about 4 times. Compared with wet machining, dry roller cutting machine processing can reduce wood processing by 45%, of which tool costs are reduced by 40%, cutting oil costs are reduced by 100%, and electricity costs are reduced by 33%; Plus the parts are of higher quality and clean and clean; No oil mist, dry chips, the working environment is improved, cleaner and safer.

The key technologies that need to be addressed to implement dry cutting technology include the following:

(1) High rolling cutting speed Generally. In dry rolling cutting processing, the speed of the high-speed steel hob line for the coating reaches 180m/min or even higher; The speed of the carbide steel hob line is required to reach 300m/min. In order to achieve this high-speed rolling cutting process, the tool spindle can generally be realized by electrospindle; For ten tables, a new design with automatic clearance elimination gear drive system is adopted to replace the traditional worm gear transmission system, LIEHHERR. The table of small and medium-sized high-speed gear hobbing machines of GLEASOIV and other companies has adopted torque servo motor technology, and the speed of the table has reached more than 800 r/min.

(2) Rapid separation of chips. Due to the high temperature, if the chip cannot quickly leave the tool, workpiece and machine tool, it is easy to cause thermal deformation and affect the machining accuracy, so the iron filings must be quickly and effectively removed. In dry roller cutting, iron filings are generally quickly left the tool and workpiece by high-speed rolling cutting of the hob. Many companies have also proposed some machine tool structure improvement schemes for chip evacuation problems, such as

accelerating the removal of iron filings with the help of gravity, and avoiding iron filings falling directly on the work table, and then assisting high-pressure cold air, which can achieve the effect of rapid and effective chip removal. Some companies also use stainless steel heat shields, one side of the stainless steel surface is smooth, easy to remove iron filings, and on the other hand, stainless steel has a small thermal conductivity coefficient, reducing the transfer of iron filings heat to the workbench and bed.

(3) High-speed hob. Hard alloy steel is used in the early stage of development of hob materials for dry roller cutting, but due to the high cost of carbide steel hobs, powder metallurgy high-speed steel hob cutters developed in recent years have a tendency to replace carbide steel hobs for dry roller cutting processing. In a research report, Liebherr compared the processing time and cost of carbide hob (Carbide) dry roller cutting, powder metallurgy high speed steel hob to SS-PM) dry roll cutting and conventional high-speed rigid hob (Canv.HSS) roll cutting. Comparative analysis of the results shows that compared with conventional processing, dry rolling cutting has a short processing time and lower cost. The use of powder metallurgy high-speed steel hobs has even better dry cutting processing effect than the use of carbide steel roller cutters.

Less chipless processing technology[39]. The process of manufacturing parts by precise forming method in mechanical manufacturing is called less chipless processing. Gear cold rolling mill is a chipless gear processing machine tool, which belongs to green processing technology. However, due to the limitation of cold forming processing characteristics, although the consumption of raw materials is saved, there are problems such as processing energy consumption, noise pollution and limited processing capacity in the processing process, and the development of its technology still needs to be vigorously promoted.

CNC technology. The numerical control transformation of gear processing machine tools is conducive to the greening of its design and manufacturing, which is mainly manifested in the following aspects.

(1) The numerical control transformation of gear processing machine tools is conducive to simplifying the mechanical structure of machine tools, thereby reducing the

consumption of raw materials for machine tools and energy accessories required for their manufacturing, saving resources and reducing environmental pollution.

(2) The use of numerical control program improves the degree of automation of the machine tool, everyone shortens the adjustment time of the machine tool, and improves the productivity.

(3) Cutting speed, feed and other cutting parameters can be adjusted arbitrarily, which improves the flexibility of processing and optimizes cutting parameters.

(4) Human-computer interactive boundary, easy to operate, and usually adopt sealing processing mode, greatly reducing the labor intensity of the operator, improving the safety of operation, conducive to labor protection.

5.3.4 Adopt effective cleaning technology for parts

These mainly include vacuum cleaning and ultrasonic cleaning. Vacuum cleaning is mainly the application of heated water, anti-rust liquid or cleaning liquid, the application of negative pressure for spraying, soaking, etc. on metal parts cleaning, rust prevention, drying, etc., the application of this method can reduce the use of lye and fluorochlorane solvent, to prevent the destruction of the atmospheric ozone layer, the technology has strong reliability, stability. Ultrasonic cleaning is mainly the use of ultrasonic waves can play a cavitation effect in the liquid, will produce very strong energy, the dirt particles on the object will peel off, the cleaning effect is good, and can play a role in accelerating dissolution and emulsification, removing the gas in the liquid.

5.4 Contamination prevention plan for parts cleaning fluid cleaning process

5.4.1 Vacuum cleaning and drying technology

In order to prevent environmental pollution in the process of parts cleaning, vacuum cleaning and drying technology can be used, that is, the solid with heated water-based cleaning liquid, clean water, anti-rust liquid, metal parts under negative pressure spraying, soaking, agitation and other ways of washing, rust prevention, drying and other treatment. Under negative pressure (vacuum), the boiling point of the cleaning mixture is lower than at normal pressure, making it easy to wash and dry. After the cleaning mixture, it can be

recycled after precipitation and oil-water separation. This method can replace lye and wash with fluorochlorane solvents to avoid damage to the atmospheric ozone layer. Vacuum cleaning technology, the role of environmental protection is pollution-free, can achieve fully automatic control, reliability and stability greatly improved, and the process is simple and flexible, equipment can be large or small, suitable for cleaning the surface of metal parts oil, especially vacuum heat treatment before cleaning and oil quenching after cleaning, cleaning quality, high efficiency, is a clean production technology.

5.4.2 Ultrasonic cleaning technology

From mechanical parts to mechanical parts, from electrical parts to electrical parts, there are cleaning requirements, such as gears, crankshafts and even gearboxes, and such as mechanical and electrical assemblies on electrical parts, and some precision mechanical parts and electrical parts, which are inseparable from cleaning. Most companies use traditional cleaning methods, such as immersion cleaning and spray cleaning. This cleaning method is not only labor-intensive, but also easy to cause environmental pollution and waste of water resources. At present, many companies have begun to use ultrasonic cleaning to eliminate the drawbacks of traditional cleaning, especially some mechanical parts with complex shapes, which are powerless by traditional cleaning methods. Ultrasonic cleaning is the use of ultrasonic cavitation in the liquid to produce a very powerful energy, peel off the dirt particles from the object, in order to achieve the purpose of cleaning; At the same time, ultrasonic waves can also accelerate dissolution and emulsification in liquid chemical reactions, and can effectively remove the gas in the liquid.

Machinery manufacturing industry is very important for industrial development, but its important part of machinery manufacturing metal machining process will cause certain pollution to the environment, this paper from the metal parts machining process to the process of parts cleaning, are implemented environmental pollution prevention measures, has a certain effect. To sum up, in the process of continuous technological progress, by making full use of it, improving the metal machining process, reducing the waste of

resources and avoiding excessive pollutants, it is conducive to the development of the manufacturing industry and avoids pollution to the environment.

Conclusion of part 5

This chapter introduces the environmental hazards that may occur in the process related to metal machining in the machinery manufacturing industry, and proposes new processing technologies to reduce environmental pollution caused by face gear processing and manufacturing.

REFERENCES

1. Zhang Juan, Wang Xiaoning. *Research status and development of gear transmission* [J]. Southern Agricultural Machinery, 2015(11):53, 55.
2. Zhu Rupeng, Pan Shengcai, Gao Deping. *Research status and development of face gear transmission*[J]. Journal of Nanjing University of Aeronautics and Astronautics, 1997(03):111-116.
3. Filler R, Heath G F, Slaughter S C, et al. *Torque splitting by a concentric face gear transmission*[C]. Candan : The American Helicopter Society 58th Annual Forum, 2002: 11-22.
4. Fu Zeshao, *New worm gear transmission*, Xi'an: Shaanxi Science and Technology Publishing House, 1990.
5. Wang Jun, Pan Wenbin. *Development of face gear transmission technology for helicopter drive systems* [J]. Aerodynamics,2018(05):44-46.
6. F.L.Litvin, Y.Zhang and J.C. Wang. *Design and Geometry of Face-gear Drive*, ASME, Journal of Mechanical Design ,1992, 114:642-647.
7. F.L.Litvin,A .Ege1jaJ,Tan and G.Heath,*Computerized Design,Generation and Simulation of Meshing of Orthogonal Offset Face-gear Drive with a Spur Involute Pinion with Localized Bearing Contact*,Mechanism and Machine Theory, January-February 1998, 33(1-2):87-102.
8. Marco Gabiccini,Massimo Guiggiani and Francesca Di Puccio,*Geometry and Kinematics of Face Gears Mating with a Helical Involute Pinion*,Proceedings of the 11th World Congress in Mechanism and Machine Science, 2004-4-14.
9. Ren Jingxin, Liu Hongzhong, Zhang Yingchang, *Gear Engineering* [M], Beijing: National Defense Industry Publishing House. 1985:232-269.
10. Gregory F.Heath,Robert R.Filler,Jie Tan.*Development of Face Gear Technology for Industrial and Aerospace Power Transmission*[R].NASA/CR—2002-211320
11. F.L.Litvin.*Application of Face Gear Drivesin Helico Transmissions* [J].Transaction of the ASM E,Journal of Mechanical Design,1994,116:672-676

12. F.L.Litvin,A.Egelja.*Handbook on Face Gear Drives with a Spur Involute Pinion* [R].NASA/CR-2000-209909
13. F.L.Litvin,Fuentes A,Zanzi C and Pontiggia M.*Design,generation, and stress analysis of two versions of geometry of face-gear drives*[J].Mechanism And Machine Theory, 2000, 37(10): 1179-1211
14. HOU LJ, LI Qing, PENG Xueyu, WU Songyong. *Parametric modeling and contact analysis of offset worm face gear transmission*[J]. Mechanical Design and Research,2016,32(01):32-36.
15. LI Qing,XU Weijun,ZHANG Meng,YANG Haixian,LIU Yunjin. *Theoretical research and practice of machining worm face gears by flying tool method* [J]. China Mechanical Engineering,2019,30(23):2835-2843.
16. Wang Shuren, Liu Pingjuan, *Principle of Cylindrical Worm Drive Meshing*, Tianjin: Tianjin Science and Technology Press, 1982
17. Fu Zeshao, *Differential Geometry and Gear Meshing Principle*, Shandong: University of Petroleum Press, 1999
18. Du Jiangge, *Offset Cylindrical Worm Drive Meshing Analysis*, Tianjin: Tianjin University,2009
19. Zhu Rupeng, Pan Shengcai, Gao Deping, *Characteristics and meshing principle of surface gear transmission*[C], Chinese Society of Aeronautics and Astronautics Proceedings of the 9th Conference on Mechanical Power Transmission, Jiangxi, 1998
20. Sheng Wei, Feng Zhanrong, Wang Lixia. *Study on root cutting of arc tooth profile gear*[J]. Mechanical Transmission, 2018, 42(06): 28-31.
21. Zhang Ce, *Mechanical Principles and Mechanical Design* (Volume I), Beijing: China Machine Press, 2004
22. Lin Qing'an, *Advanced Part Design* (I), Beijing: Tsinghua University Press, 2003, 145-172
23. "Working Principles of Teeth Grinding", Working Principles of Teeth Grinding, Beijing: China Machine Press,1977,69-87

24. Jin Guanghu. *Analysis and study on strength and dynamic characteristics of orthogonal gear transmission*[D]. Nanjing University of Aeronautics and Astronautics, 2012.
25. Litvin F L. *Gear geometry and application theory*[M]. Guo Kai, Ye Lingyun, Fan Lin, et al. trans. Shanghai: Shanghai Science and Technology Press, 2008.
26. XU Zhilun. *Elasticity*[M]. Beijing: Higher Education Press, 1990.
27. Quan Yongxin, Shi Gaoyi. *Principle of friction and wear*[M]. Zhejiang: Zhejiang University Press, 1986.
28. CHEN Fengqiong, HUANG Jin, DENG Huixin, RAN Ruihong. *Occupational and Health*,2021,37(22):3028-3032.DOI:10.13329
29. LIU Jinyan, GONG Guozhuo, LIU Hongjuan. *Modern Occupational Safety*,2019(05):86-88.
30. LI Feihui, TANG Yuqiao, CHENG Shuqun. *The impact of occupational disease hazard factors on workers' health in automobile manufacturing industry*[J].Occupational Health,2017
31. Pan Yanjun. *Occupational hazards and prevention and control measures in automobile manufacturing industry*[J].Modern Occupational Safety,2017(04):96-98.)
32. Zhang Huiqin. *Discussion on occupational hazards in machinery manufacturing industry and their prevention and control countermeasures*[C]//. 2016:51-53.
33. Wang Yongzhuang. *Exploration of fire prevention inspection and fire hazard rectification method*[J]. Fire Protection (Electronic Edition),2022,8(16):90-92.
34. Shangguan Xiangfei. *Study on fire causes and fire safety of high-rise buildings*[J]. Fire Protection Today,2021,6(10):133-135.
35. Xie Menglu. *Research on the impact of manufacturing agglomeration on environmental pollution*[D].Nanjing University of Science and Technology,2021.
36. *Rare metal processing and environmental pollution*[J]. Rare Metal Alloy Processing, 1979, (06): 1-9.
37. Li Maosheng. *Development and development trend of green metalworking oil*[A]. Chinese Mechanical Engineering Society,2004:154-160.

38. HU Guiling. *Research on dry cutting technology in green cutting*[J].Shihezi Science and Technology,2021(06):39-40.)

39. NIU Yongsheng,YU Haiyun,MENG Lingjun. *Application of chipless chipless processing technology in automotive transmission parts*[J].Mechanical Transmission,2005(04):75-77.DOI:10.16578